ELSEVIER

Polymer 40 (1999) 6729–6751

polymer

Finite strain behavior of poly(ethylene terephthalate) above the glass transition temperature

P.G. Llana, M.C. Boyce*

Department of Mechanical Engineering, Massachusetts Institute of Technology, Cambridge, MA, USA

Received 19 August 1998; received in revised form 28 November 1998; accepted 10 December 1998

Abstract

An experimental study of the strain rate and temperature dependencies of the stress–strain behavior of PET under large strain deformation was conducted over a range in strain rates (-0.005 to $-2.0\,s^{-1}$) and temperatures (90°C–105°C) in both uniaxial and plane strain compression. The increase in crystallinity content with varying strain rate and temperature and for the two different states of strain that developed as a result of these deformation conditions was investigated using Differential Scanning Calorimetry (DSC). The nature and evolution of the crystallographic texture was studied using Wide Angle X-ray Diffraction (WAXD) measurements. The stress–strain behavior is found to exhibit four characteristic features: (1) a relatively high initial stiffness, (2) followed by a rollover in the stress–strain curve to flow behavior, (3) followed by an increase in stress with continuing strain, (4) followed by a dramatic increase in stress with strain at very large strains. These four features strongly depend on strain rate, temperature and state of strain. DSC and WAXD measurements on deformed specimens indicated an increase in crystallinity with increasing strain rate and decreasing deformation temperature under both uniaxial and plane strain conditions. The WAXD measurements also revealed that the preferential crystallographic texture that develops is consistent with the molecular orientation which develops with the different states of strain.

Keywords: Stress–strain behavior; Strain-induced crystallization; Poly(ethylene terephthalate)

1. Introduction

Poly(ethylene terephthalate) is a thermoplastic polymer found in numerous commercial applications and is typically processed in the solid state at temperatures in or above its glass transition temperature, T_g, by blow molding, vacuum forming, drawing, or biaxial stretching. These stretching processes act to preferentially orient the underlying macromolecular structure producing either an oriented amorphous state or an oriented semicrystalline state. Indeed, PET exhibits the capability of undergoing crystallization during stretching. This phenomenon is often termed strain-induced or stress-induced crystallization. The result of strain-induced crystallization is increased stiffness and hardness as well as better dimensional stability, also referred to as resistance to recovery.

There were numerous investigations on the mechanical behavior of PET owing to its wide range of applications. Its commercial success is mainly owing to its ability to undergo strain-induced crystallization at various stretching rates, states, and temperatures. This strain-induced crystallization is also a primary reason for the inability to accurately predict its behavior during processing. The purpose of this paper is to present a systematic study of the effects of strain rate, temperature and state of strain on the large strain mechanical behavior of PET and the corresponding evolution in structure with strain at temperatures above the glass transition. A brief review of relevant work of others is first presented. Details in the experiments which sample the mechanical behavior of PET under different states of large strain, over a wide range of strain rates, and over a range of temperatures above the glass transition temperature are then given. Differential Scanning Calorimetry (DSC) measurements are utilized to estimate the crystallinity content as a function of mechanical loading (strain state, strain rate, final strain, temperature). Wide Angle X-ray Diffraction (WAXD) is then used to determine the nature of this crystallinity and the development of texture with strain state, strain rate, final strain and deformation temperature.

2. Background

Over the years, investigators have studied PET in view of

* Corresponding author. Tel.: +1-617-253-5353; fax: +1-617-258-8742.

0032-3861/99/$ - see front matter
PII: S0032-3861(98)00867-2

either understanding its crystallization behavior and/or its mechanical behavior [1–9]. The most directly relevant of these works is discussed later and, as will be shown, a picture begins to emerge regarding the effects of temperature, strain rate and state of deformation on the mechanical and microstructural evolution in PET with deformation.

In work on "stress-induced" crystallization, Misra and Stein [6] investigated the microstructure of quenched amorphous PET films stretched both below and above T_g by performing density measurements, small angle light scattering, and wide angle X-ray scattering measurements. In this study the strain rate (300% min^{-1}) was not changed while the temperature and the amount of strain were varied. Considerable crystallinity was found to occur with stretching and the percent crystallinity increased when stretching was followed by annealing. It was found that for samples stretched at 80°C an increase in crystallinity was observed only beyond 80% nominal strain. This increase in crystallinity rose with increasing nominal strain, for example from 4% to 13% to 21% crystallinity at nominal strains of 80%, 200%, and 300%, respectively, and levelled off at higher strains ($\backsim$ 380% strain).

Porter and co-workers [7,8] have conducted extensive tests on the deformation of PET and poly(ethylene-2,6-naphthalate) (PEN) and have subsequently investigated the effects of extent of deformation and deformation temperature on the material microstructure. Ghanem and Porter [7] conducted isothermal solid-state coextrusion experiments on isotropic amorphous PEN both below and above its T_g and studied the behavior of the onset of cold crystallization (T_{cc}) with respect to extrusion temperature (ET) and extrusion draw ratio (EDR). DSC analysis showed that the T_{cc} decreased markedly with increasing EDR and goes through a minimum in the vicinity of the glass transition region. It was found that the percent crystallinity induced by draw, calculated from DSC analysis, increased continuously with increasing EDR and with increasing ET from 5% to 35% crystallinity. After this increase the crystallinity then reached a saturation value which was about 35% for an EDR of 2.3 at an ET of 150°C. Guan et al. [8] performed planar deformation of amorphous PET in equi-biaxial stretching and forging at temperatures above T_g (80°C–100°C) and monitored the evolution of crystallinity with DSC, WAXD, density and elastic recovery measurements. It was found that, at a temperature of 90°C, as the biaxial draw ratio increases, the area of the cold crystallization exotherm decreases. This is a manifestation of the presence of strain-induced crystallization owing to large deformations. They also observed that the percent crystallinity, as measured by WAXD, decreased as the stretching temperature was increased in biaxial stretching. This was attributed to the thermal relaxation process, which is competing with the chain orientation process, becoming more pronounced as the deformation temperature increases from T_g, and thus hinders crystallization. What was also shown was that the orientation and crystallization obtained from equi-biaxial stretching and uniaxial compression is essentially identical, as the only difference observed could be attributed to an effect of strain rate, which they were unable to maintain constant during their tests.

Jabarin and co-workers [9,10] have extensively investigated strain-induced crystallization in the rubbery region. The mechanical behavior of simultaneous and sequential biaxial stretching of initially amorphous PET films at temperatures ranging from 80°C to 110°C, nominal strain rates ranging from 5% to 200% s^{-1} and extension ratios from 4 to 5 (which correspond to a tensile logarithmic strain of 1.38–1.6) was found to depend on the deformation temperature and strain rate. Crystallinity was measured using DSC and was also studied, in some cases, using small angle light scattering and WAXD. Their results are consistent with the findings of Misra and Stein [6] and also Porter and co-workers [7,8] with respect to strain-induced crystallization. The crystallinity was found to develop a rod-like fibrillar structure depending on the extent of stretching. Mechanically, the strain-induced crystallization can be observed by a noticeable increase in strain hardening that starts at a temperature and strain rate dependent level of strain. They call this strain the strain hardening parameter (SHP). They do, however, state that some crystallization does occur prior to SHP. When deformation is slow, strain-induced crystallization does not occur and is considered to be owing to molecular relaxation having time to occur which inhibits orientation and subsequent crystallization. Mechanically, the strain hardening is very low or not present at all in these cases. This molecular relaxation phenomenon is consistent with the finding of Porter and co-workers [7,8]. This rate effect on strain-induced crystallization is very important with regard to understanding and being able to predict the mechanical behavior during processing. The work conducted by Jabarin [9] indicates that the rate effect is larger over the strain rate range examined as the temperature increases. However, if the strain rate is high enough at a given temperature, the strain hardening is nearly independent of rate. Chandran and Jabarin [10] also found the presence of a strong dependence of the strain state history on both crystallization and strain hardening. It was found that the stress-strain curves for specimens stretched in the simultaneous biaxial mode were always concave upward. In contrast, when stretching in the sequential mode, the stress–strain curve from the second stretch would be convex upward or concave upward when the initial stretch level was greater than the SHP or less than the SHP, respectively.

Buckley and co-workers have also conducted several studies on PET [11–13]. Buckley et al. [11] report on both uniaxial and constrained width (plane strain) drawing tests on PET film above T_g (75°C–120°C) at nominal strain rates ranging from 1 to 16 s^{-1} on a flexible film tester. The crystallinity content in the deformed specimen was monitored using density measurements. The stress–strain behavior was found to exhibit an initial yield-like behavior

which depended on strain rate followed by an increase in stress with strain (strain hardening) which did not show any strong rate dependence in the reported data. The yield and hardening behavior were found to strongly depend on temperature, where hardening rate decreases with increasing temperature. There was not a very large difference in strain hardening between uniaxial and constrained width stretching. This was attributed to the similar molecular orientations obtained in these two stretch states. Adams et al. [12] investigated the yield stress dependence on the strain-rate ratio during biaxial hot-drawing of amorphous PET at 87°C. With a nominal strain-rate of 1 s^{-1} in the 1-direction, it was found that the yield stress in the 2-direction increased with increasing strain-rate ratio. Also, the strain hardening behavior exhibited a more dramatic upturn as the strain-rate ratio was increased.

Salem [14] studied the evolution of crystalline order during drawing of PET at 90°C and at nominal strain rates in the range 0.01–2.1 s^{-1}. Salem found that the onset of crystallization always occurred at the inflection point in the stress–strain curve, which shifts to higher strain levels and lower stress levels as strain rate decreases. Salem found the crystallinity to develop in two regimes: in the low stress regime (1) crystallinity increases more rapidly than in the high stress regime (2). The onset of regime (2) occurs in the region of the sharp upturn in the stress–strain curve at a characteristic level of crystallinity which is independent of strain rate. WAXD determinations of the lateral crystallite dimensions normal to the (0 1 0) and (1 0 0) planes revealed that crystallization in regime (2) involved modest growth of crystallites with preferential growth occurring normal to (0 1 0).

In a recent work, Zaroulis and Boyce [15] studied the mechanical and crystallization behavior of PET over a wide range of strain rates (0.005–0.5 s^{-1}) and temperatures (25°C–80°C) in both uniaxial and plane strain compression conditions. A dramatic drop was observed in both modulus and yield stress with temperature, accompanied by a drop in percentage softening after yield. The strain hardening was found to be relatively independent of temperature over this temperature regime. DSC conducted on the deformed and undeformed samples show that the cold crystallization temperature decreases with strain and this occurs to a greater extent at higher temperatures of deformation. Comparison of the areas of these exotherms with the melt endotherm indicated, however, that there was no change in crystallinity content over this temperature range for material deformed by uniaxial compression. It was concluded that for uniaxial compression, the strain hardening in this temperature regime is owing to molecular orientation and not crystallization. However, DSC revealed that crystallization occurred during plane strain compression, which indicated that strain hardening during plane strain may be owing to both orientation and crystallization. Additional experiments conducted at 80°C showed a dramatic change in the strain hardening behavior. At low strain rates (0.005 s^{-1}), the strain hardening behavior at 80°C is lower than that observed in the range of 60°C–76°C. At high rates (0.5 s^{-1}), however, the hardening is dramatically higher. These results are consistent with the investigations of Porter and co-workers [7,8] and Jabarin and co-workers [9,10], which indicate that at longer times and higher temperatures, a network relaxation occurs, while at higher rates, orientation does not have time to relax and therefore crystallization occurs.

Blundell and co-workers [16,17] have recently reported intriguing in situ measurements on structural changes during fast uniaxial drawing of PET by capturing simultaneous wide angle X-ray scattering patterns using synchrotron radiation. Drawing was studied at 80°C, 90°C, 100°C, and 110°C to a final draw ratio of $\backsim$4.1 at a nominal draw rate of $\backsim$10 s^{-1}. They found that, at these drawing rates, essentially all crystallization occurred in a very short period ($\backsim$500 ms) after final extension was achieved and that crystallization does not occur below a critical draw ratio. This critical draw ratio is in the range 1.4–2.5, increasing with deformation temperature. After this critical draw ratio was reached, the percent crystallinity increases with draw ratio. These results suggest that the crystallization measurements of others on specimens after deformation may be measuring crystallization that occurred during the time after straining was completed as opposed to that which occurred during straining. On the surface, this result implies that the strong strain hardening response that many others attribute to crystallization does not correlate with crystallization as strain hardening occurs during straining and crystallization apparently does not occur during active straining at these high rates. However, this is a rather simplistic interpretation as it does not account for the role of the highly ordered oriented amorphous domains which must immediately precede crystallization. Therefore, although post-deformation crystallization measurements may not necessarily indicate that crystallization occurred during active straining, they may still reflect the formation of highly ordered oriented domains during deformation.

From the previous review [16,17], it is apparent that a comprehensive set of mechanical tests with subsequent microstructural analysis on the deformed material can provide a picture of the mechanical and structural evolution of PET. Although the studies described begin to determine the complex connection between deformation, time, temperature and crystallization, they have not individually spanned a range of homogeneous deformation states, rates of stretching, and temperatures. Increasing the extent of deformation acts to orient the molecular network, which, under favorable conditions such as high strain rates and temperatures, leads to strain-induced crystallization. This work builds on the work conducted by others and examines the mechanical behavior of initially amorphous PET in the rubbery region where there is a balance between strain-induced crystallization at high rates as well as network relaxation at low rates, as suggested by several investigators

[8–15]. The experimental part of this investigation, which consists of mechanical tests and microstructural analysis using DSC and WAXD, is presented later and serves as a basis for the constitutive modeling that is presented elsewhere.

3. Experiments

3.1. Material/specimen description

The material used in the experiments is nearly amorphous isotropic PET, with molecular weight $\bar{M}_w = 49\,700$. The PET was in sheet form and was supplied by Eastman Kodak Company. The material sheets, whose average thickness is 2.09 mm, appear optically clear, implying a low crystallinity content. DSC measurements of the as-received material indicated a residual crystallinity content of about 10%. WAXD scans did not reveal any crystalline peaks indicating a purely amorphous material. There is typically some level of discrepancy between DSC and WAXD measurements of crystallinity. The WAXD data more distinctly detects the presence of crystallinity; however, the DSC scans serve to provide a relative comparison for differences in percentage crystallinity after different amounts of strain.

Uniaxial and plane strain compression tests were conducted in order to explore the mechanical behavior of the material. Compression tests were chosen over tension tests because it is relatively easy to achieve a controlled homogeneous deformation in compression with very small variations in specimen temperature. In previous compression tests on thermoplastics conducted by Arruda and Boyce [18] test specimens were machined from bulk and the tests were conducted using Teflon sheets as a lubricant between the specimen and the compression platen surface, which proved to provide excellent conditions for obtaining homogeneous deformations thereby resulting in accurate true stress vs. true strain data. In the work by Zaroulis and Boyce [15], PET sheets of similar dimensions ($\backsim$1.73 mm thickness) were used. It was found that the relatively small thickness of the specimens posed a problem of specimen size, particularly when considering that the material was compressed to a true compressive strain of -1.75, which causes a height reduction of the order of 85%. Zaroulis and Boyce found that an initial height to diameter ratio of 0.5 or larger gave repeatable results. In order to provide a test specimen of reasonable height, a stack of three disks was needed to make one uniaxial compression specimen. To achieve the 0.5 initial height to diameter ratio, disks of 12.38 mm diameter were machined from the PET sheets. Also, to eliminate the possibility of slippage between the disks for the duration of the experiment, the two disk–disk interfaces were roughened with coarse grid sand article. To reduce the amount of friction between the disk-compression platen interfaces, Teflon sheets and a common lubricant, WD40, were used. In order to avoid the possibility of WD40 coming between the disks, the WD40 was only sprayed between the Teflon sheets and the compression platens.

Plane strain compression specimens were machined in a similar manner. Each plane strain compression specimen consisted of a stack of three squares. The squares were machined from the PET sheets with sides measuring 9.55 mm. The initial height to width ratio for these specimens were approximately 0.65. The plane strain compression specimens were found to give nearly homogeneous deformations to a final true strain of -1.6.

3.2. Description of mechanical tests

Uniaxial and plane strain compression tests over a range of strain rates and temperatures were conducted in order to measure the stress vs. strain behavior of PET. The temperature range spans from 90°C to 105°C where the glass transition temperature, T_g, is approximately 79°C. The strain rate range spans from the slow isothermal rate of $-0.005\ s^{-1}$ to the fast nearly adiabatic rate of $-2.0\ s^{-1}$.

The mechanical tests were performed on an Instron 1350 servohydraulic machine using a Pentium computer running LabVIEW, a common data acquisition and control software package. The tests were performed in the strain control mode with a 2620-824 Instron extensometer in order to eliminate the Instron load train compliance errors and obtain the best accuracy in the measurement of deformation at high levels of true strain. Following Hasan and Boyce [19], for the duration of each experiment, logarithmic strain was monitored as a function of time and fed back to the controller in order to alter the actuator displacement rate to provide constant strain rate conditions. Due to the strong rate dependence of various aspects of the material behavior, constant strain rate conditions are desirable. For example, a nominal rate of $1\ s^{-1}$ at the beginning of a tensile stretch test is reduced to an actual rate of $0.25\ s^{-1}$ at a stretch ratio of 4.

For the elevated temperature experiments, a radiant furnace was used to bring the sample to the desired experimental temperature. The time required for the environment of the furnace to reach thermal equilibrium was between 15 and 20 min. There was concern that this “equilibrating time” might induce crystallization in the specimens even before compression. This was determined not to be the case by conducting a DSC scan on a specimen that had been heated in the furnace for the same time duration but not deformed. In the uniaxial compression experiments, the specimen temperature was monitored with four type-K thermocouples. Two thermocouples were cemented to both the top and bottom compression platen, with all four thermocouples spaced evenly about the circumference of the platens 90° apart. In the plane strain compression experiments, only one thermocouple was used, which was positioned inside the channel die fixture in contact with the specimen. The fact that the lower actuator head gets cooled

Table 1
Comparison of heat transfer conditions at different strain rates for uniaxial and plane strain compression experiments

Strain rate	Uniaxial		Plane strain	
$\dot{\varepsilon}$ (s^{-1})	t_{exp}/t_{cond}	Heat transfer condition	t_{exp}/t_{cond}	Heat transfer condition
−0.005	40.7	Isothermal	32.5	Isothermal
−0.01	20.3	Isothermal	16	Isothermal
−0.05	4.1	Coupled	3.25	Coupled
−0.1	2.0	Coupled	1.63	Coupled
−0.5	0.41	Coupled	0.33	Coupled
−1.0	0.20	Coupled	0.16	Coupled
−1.5	0.13	Adiabatic	0.11	Adiabatic
−2.0	0.10	Adiabatic	0.08	Adiabatic

by the actuator fluid caused a temperature difference to develop between the two compression platens that manifested itself if the furnace was used for an extended period of time. This temperature difference was allowed to be no more than 2°C above or below the target temperature, at which point the testing was stopped and the upper actuator head allowed to cool.

Owing to the range of the strain rates utilized in these experiments, the actual duration of the experiments varied from approximately 0.8 s for the $-2.0\ s^{-1}$ rate, to 400 s for the $-0.005\ s^{-1}$ rate. The inelastic nature of the deformation results in heat dissipation that may or may not produce a temperature rise in the specimen during the test, depending on the strain rate and the experimental temperature of the test. Obviously, the faster the rate of the experiment, the less time for heat transfer, thus the more important the heating effects. Also, the higher the temperature, the smaller the value of the plastic work input to the sample, and hence the lower the temperature rise owing to deformation. In this work, an experiment is classified as isothermal, thermomechanically coupled, or adiabatic by comparing the duration of the loading part of the experiment, t_{exp}, to the time required for the conduction of heat out of the specimen, t_{cond}. The first order analysis used to determine this classification is given in the appendix.

Table 1 shows the heat transfer calculations for both uniaxial and plane strain compression experiments. It can be seen that the experimental time is much longer than the conduction time for the -0.005 and $-0.01\ s^{-1}$ rates, hence the heat transfer conditions during those experiments are expected to be isothermal. Similarly, as the experimental time is about as long as the conduction time for the -0.05, -0.1 and $-0.5\ s^{-1}$ rates, the heat transfer conditions during those experiments are expected to be thermomechanically coupled. Lastly, as the experimental time is much shorter than the conduction time for the $-1.5\ s^{-1}$ strain rate and faster strain rates, the heat transfer conditions during these experiments are expected to be essentially adiabatic.

The temperature rise of the specimen for both the uniaxial and plane strain case for a fully adiabatic strain rate is a function of the strain. This temperature rise can be estimated by two methods using the true stress and true strain measured by the mechanical testing machine. The first method considers the entire work to be dissipative:

$$\Delta T_1 = \frac{1}{\rho c_p} \int_0^{\varepsilon_f} \sigma\varepsilon \, d\varepsilon. \quad (1)$$

The second method considers the orientation hardening to be stored energy [2] and is a function of the initial yield stress, σ_{y0}, and strain:

$$\Delta T_2 = \frac{1}{\rho c_p} \int_0^{\varepsilon_f} \sigma_{y0}\varepsilon \, d\varepsilon \quad (2)$$

where ρ and c_p are the density of amorphous PET and the specific heat capacity, respectively, as given earlier. For these two methods, in uniaxial compression at 90°C, the approximate temperature rise owing to adiabatic heating is 7°C for the first method and 1.5°C for the second method. It is also important to note that the exothermic nature of the crystallization that may be occurring with strain is also not taken into account. An increase in crystallinity from 5% to 31% would result in a temperature rise of about 14°C and may occur over a very narrow range in strain. Therefore, under coupled and adiabatic conditions, the increase in temperature plays a role in the observed mechanical response.

3.3. Description of DSC measurements

DSC was used to monitor the rate of change of specimen enthalpy as a function of increasing temperature at a given heating rate. Following [21], DSC scans were performed at a rate of $10°C\ min^{-1}$. DSC specimens with masses ranging from 3 to 10 mg were cut from the center of the deformed specimens using an Buehler Isomet low speed saw. Care was taken not to impart additional deformation to the specimens as they were cut.

DSC thermograms were taken on the as-received material as well as on the specimens deformed at different strain states, strain rates and temperatures in order to assess the effects of deformation conditions on crystallization. For all DSC thermograms, the strain level referenced for each thermogram refers to the applied strain in the corresponding mechanical compression test. Data are presented in terms of the cold crystallization temperature, T_{cc}, and the percentage

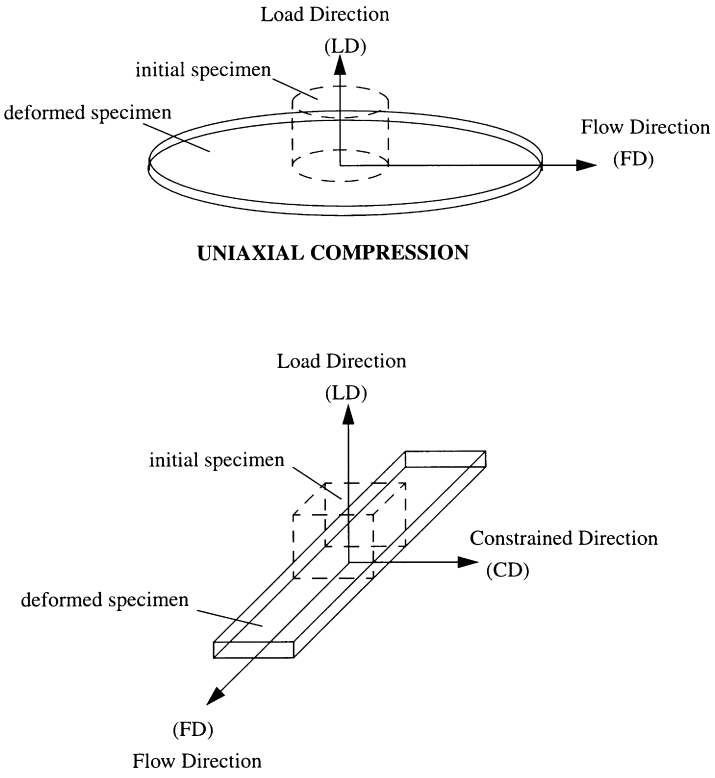

Fig. 1. Schematics of uniaxial compression and plane strain compression illustrating load, flow, and constrained directions.

crystallinity. Based on a two-phase (crystalline–amorphous) peak area method [22], the weight percent crystallinity of the material can be estimated. The weight percent crystallinity, p_{cr}, is given by:

$$p_{cr} = \frac{\Delta H_m - \Delta H_{cc}}{\Delta H_f} \tag{3}$$

where ΔH_{cc} is the enthalpy released during cold crystallization, ΔH_m is the enthalpy required for melting and ΔH_f is the enthalpy of fusion of PET crystals, taken to be equal to 120 J g^{-1} [15]. Eq. (3) gives an initial crystallinity for the as-received material of about 10%. This value for the crystallinity is inconsistent with the WAXD scan of the as-received material, which will be shown later. In the WAXD scan, there were no crystalline peaks, indicating no crystallinity in the as-received material.

3.4. Description of wide angle X-ray diffraction measurements

WAXD was used to analyze the structure and morphology developed in the specimens owing to deformation. A Rigaku RU200 185 mm CuKα rotating anode diffractometer was used to perform the X-ray diffraction measurements. Equatorial scans were conducted in the range $2\theta = 10°–50°$ with intensity data collected every 0.1° for a period of 1 s. As the deformation of the uniaxial compression specimens is axially symmetric, only two X-ray scans were performed on these specimens, whereas three scans were performed on the plane strain compression specimens, as shown in Fig. 1. For uniaxial compression specimens the first scan was conducted in transmission, with the X-ray beam positioned perpendicular to the plane of the specimen (flow direction, FD), and the second scan in reflection, with the X-ray beam positioned at a glancing angle to the plane of the specimen (load direction, LD). For the plane strain compression specimens, the first scan was conducted in transmission, with the X-ray beam positioned perpendicular to the plane of the specimen and the specimen positioned in order to sample the constrained direction (CD). The second scan was also in transmission, with the X-ray beam also perpendicular to the plane of the specimen but with the specimen positioned in order to sample the FD. The third scan was performed in reflection, with the X-ray beam positioned at a glancing angle to the plane of the specimen in order to sample the LD. For all WAXD measurements, the strain level referenced for each scan refers to the applied strain in the corresponding mechanical compression test.

4. Experimental results

Results from the mechanical tests, the DSC measurements, and the WAXD measurements are presented here.

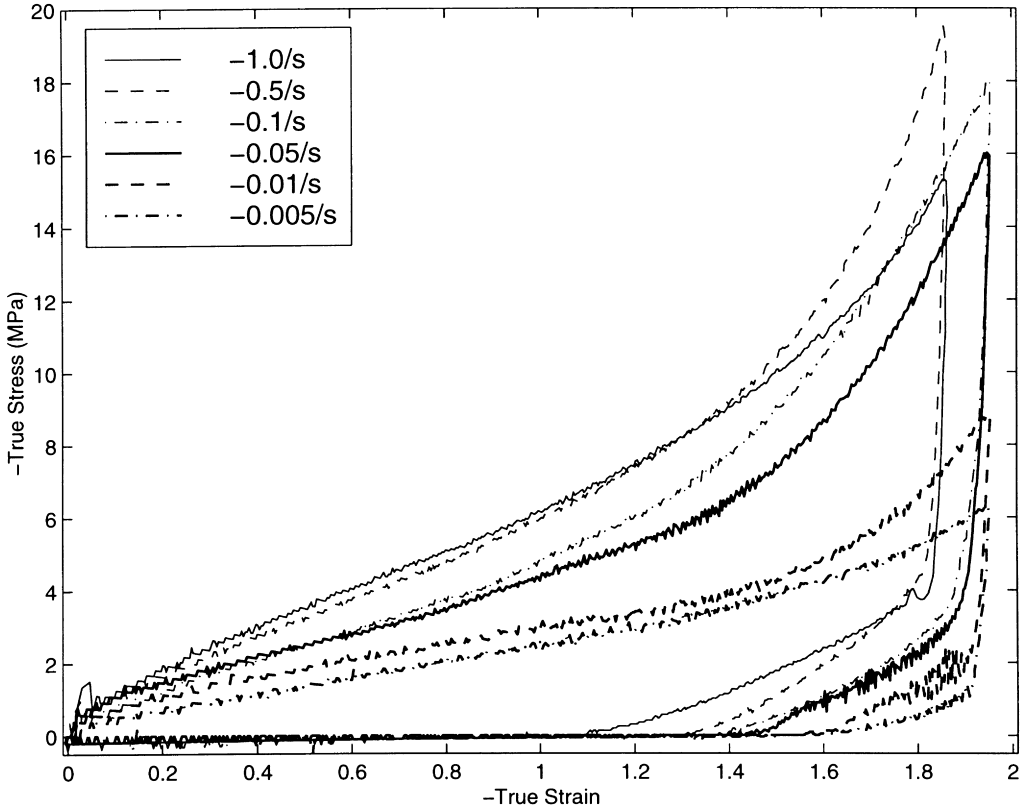

Fig. 2. True stress–strain behavior in uniaxial compression at 90°C at different strain rates.

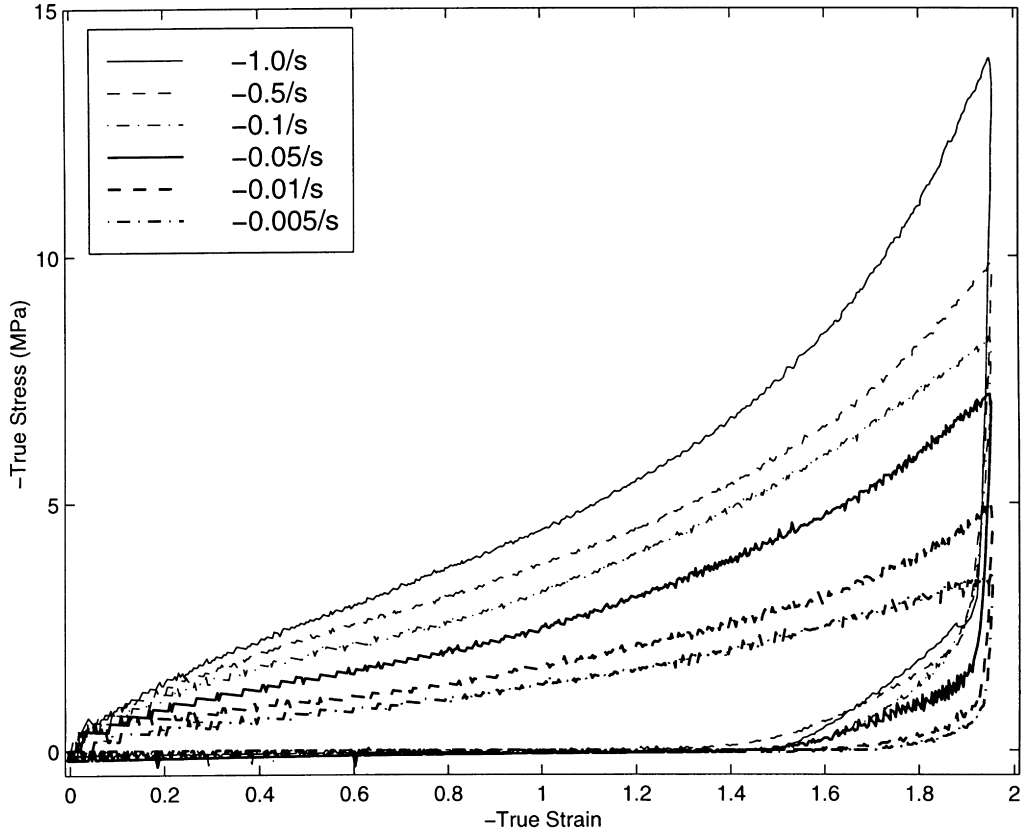

Fig. 3. True stress–strain behavior in uniaxial compression at 100°C at different strain rates.

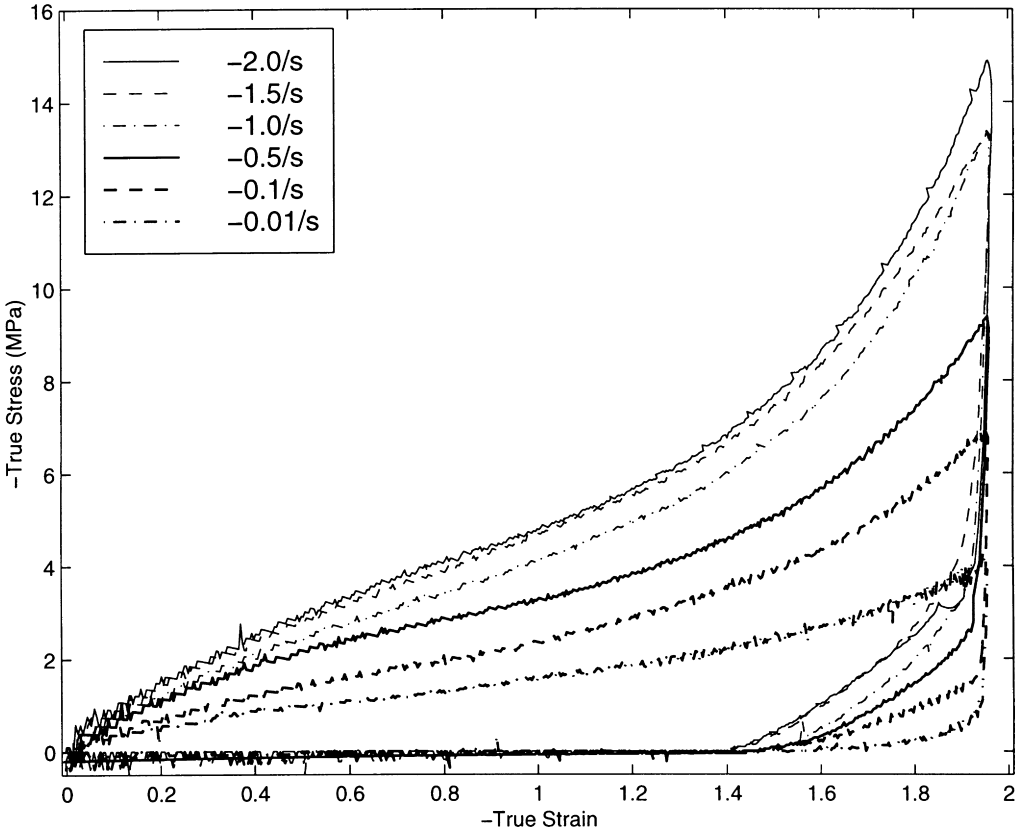

Fig. 4. True stress–strain behavior in uniaxial compression at 105°C at different strain rates.

Effects of strain rate, temperature and strain state are discussed separately for the uniaxial and plane strain mechanical tests. Cold crystallization phenomena and percent crystallinity are discussed for the DSC measurements. Evolution of crystallinity, size and number of crystallites are explored for the WAXD measurements.

4.1. Results from mechanical tests

Uniaxial compression and plane strain compression tests were conducted at temperatures of 90°C–105°C and strain rates of -0.005 to $-2.0\ s^{-1}$. Several tests were conducted at each testing condition to verify repeatability. The results of these tests are plotted in terms of true stress vs. true strain. The true strain, ϵ, is defined as the natural logarithm of the current height, h, to the initial height, h_0, given as follows:

$$\varepsilon = \ln(h/h_0). \tag{4}$$

The true stress is the ratio of the current force to the current area:

$$\sigma = F/A \tag{5}$$

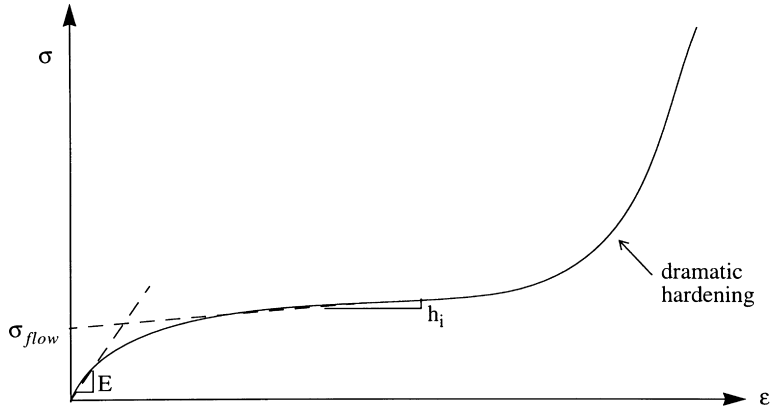

Fig. 5. Schematic of stress–strain behavior labelling significant features.

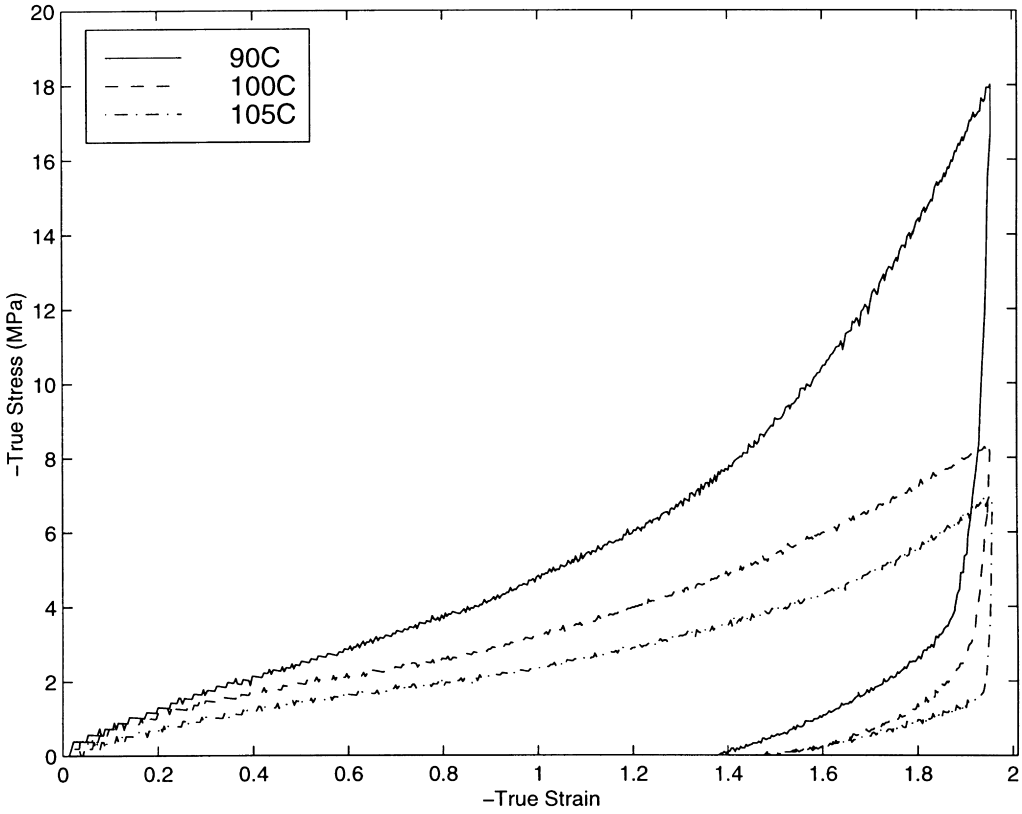

Fig. 6. True stress–strain behavior in uniaxial compression at 90°C, 100°C, and 105°C at −0.1/s.

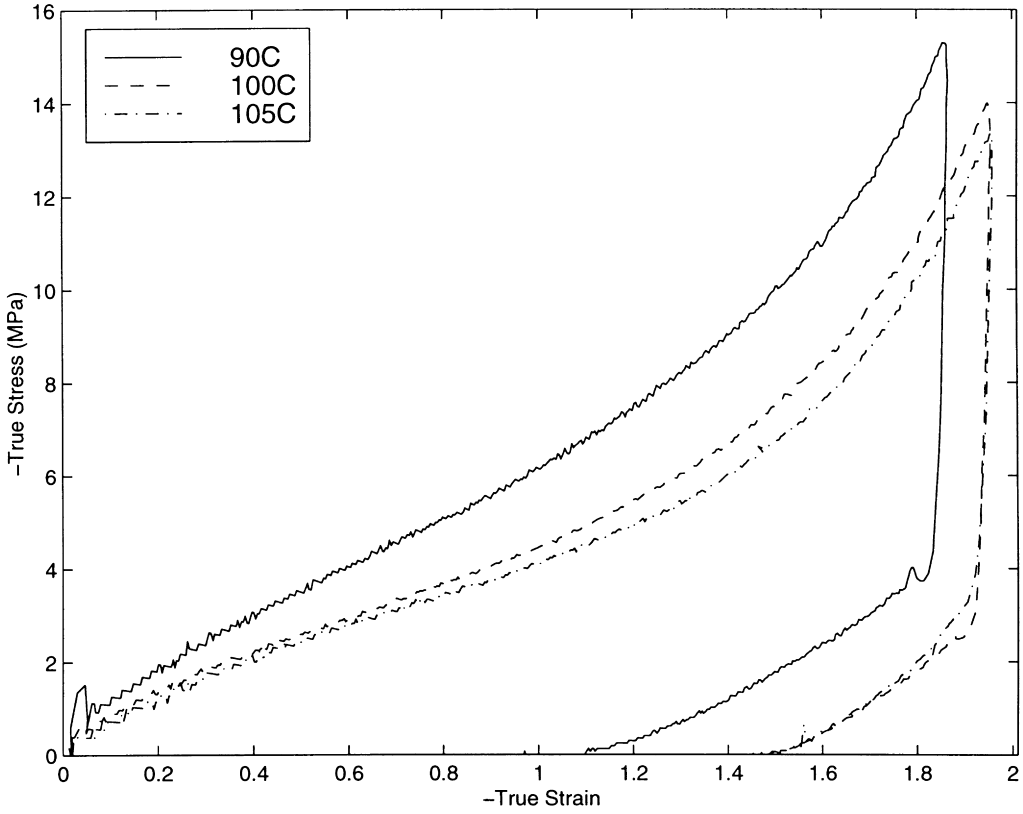

Fig. 7. True stress–strain behavior in uniaxial compression at 90°C, 100°C, and 105°C at −1.0/s.

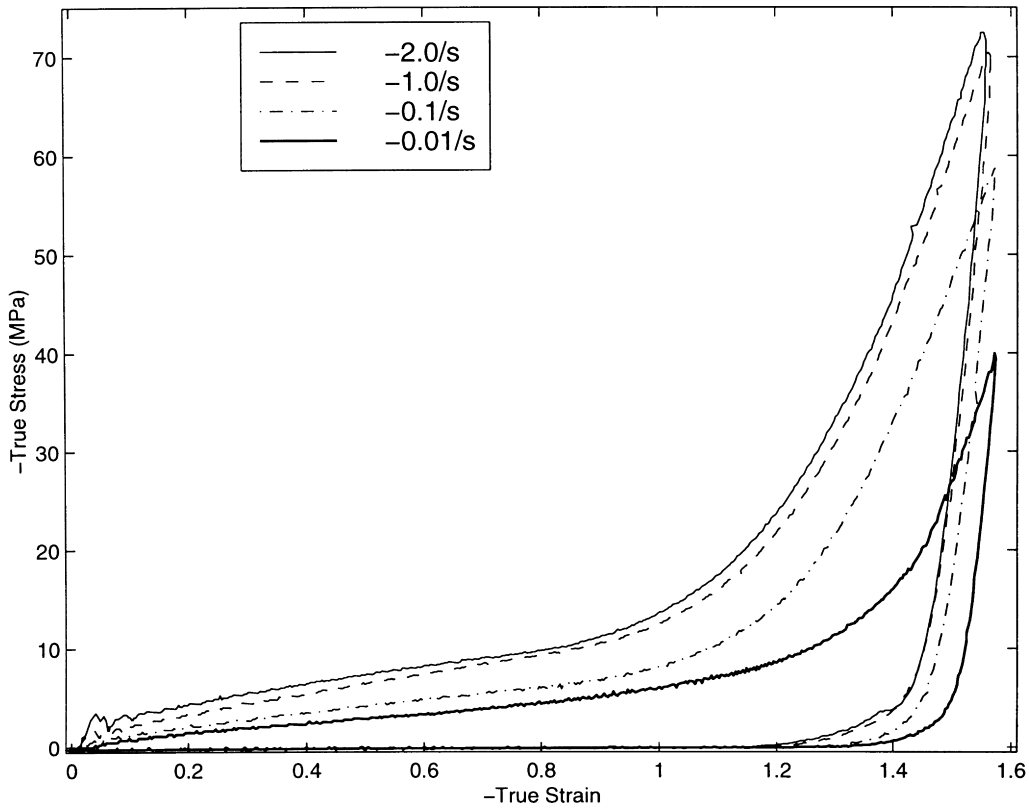

Fig. 8. True stress–strain behavior in plane strain compression at 90°C at different strain rates.

where the current area is calculated using the measured current height and assuming incompressibility of inelastic deformation.

4.1.1. Uniaxial compression tests

Figs. 2–4 show the uniaxial compression loading–unloading curves at different strain rates at a temperature of 90°C, 100°C, and 105°C, respectively. The uniaxial compression tests were conducted to a final strain of −2.0.

As previously mentioned, the glass transition temperature, T_g, for this material is about 79°C as determined by DSC. Therefore, at these test temperatures of 90°C, 100°C, and 105°C, the material is well into the rubbery region. However, the strain rate and temperature dependent nature of the material is not characteristic of classical rubbery behavior. The stress–strain behavior exhibits four characteristic features as shown in the schematic of Fig. 5: a relatively stiff initial response, followed by a rollover to a yield or flow-like behavior, followed by a gradual increase in stress with strain which is termed the initial strain hardening response, followed by a dramatic increase in stress with strain at large strains.

The strain rate dependence of the mechanical behavior can be seen in Figs. 2–4. At all three deformation temperatures, the flow stress increases with increasing strain rate. The initial strain hardening slope increases as the strain rate is increased and the strain at which dramatic hardening occurs decreases with increasing strain rate. Also, as seen in Figs. 2–4, the amount of strain hardening increases with increasing strain rate when the rates are isothermal, but as the tests become more adiabatic the strain hardening slope decreases at large strains. Therefore, at a given deformation temperature, the amount of strain hardening increases as the strain rate increases for isothermal tests. But as the tests become more adiabatic and there is less heat conducted out of the specimen to the platens, the apparent amount of strain hardening decreases owing to the simultaneous occurrence of thermal softening. These findings prove to be consistent with the first order analysis presented earlier. When comparing Fig. 2 with Figs. 3 and 4, it can be seen that adiabatic heating has more of an effect at deformation temperatures of 90°C than at 100°C and 105°C. This is as expected as the adiabatic softening contribution decreases with increasing deformation temperatures.

In this "rubbery" regime, the "yield" or flow stress is only on the order of 1 MPa. The most distinct difference between the rapid rates (−2.0, −1.5, −1.0, −0.5, −0.1, and $-0.05\,s^{-1}$) and the slow rates (−0.01 and $-0.005\,s^{-1}$) occurs in the strain hardening behavior. The behavior at the high strain rates exhibits large strain hardening suggesting the presence of strain-induced crystallization or at least more effective molecular orientation. The decrease in hardening slope with decrease in strain rate suggests a molecular relaxation process. These results are consistent with the experimental observations of Chandran and Jabarin [10].

Figs. 6 and 7 show uniaxial compression in the rubbery

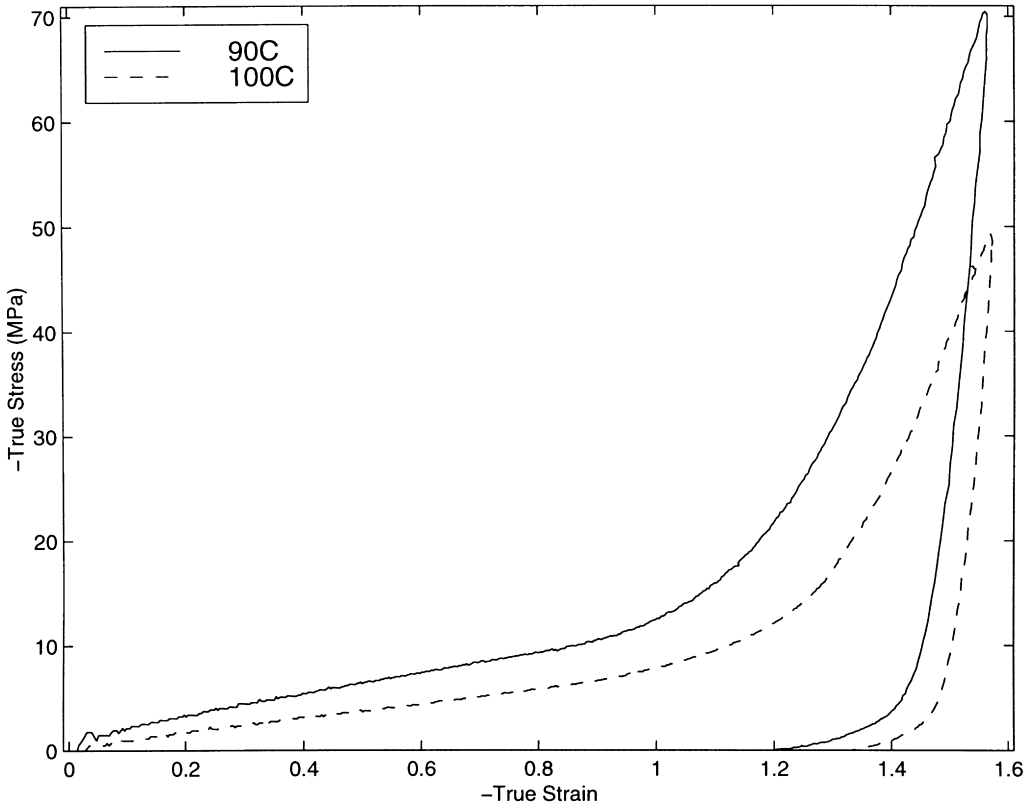

Fig. 9. True stress–strain behavior in plane strain compression at 90°C and 100°C at −1.0/s.

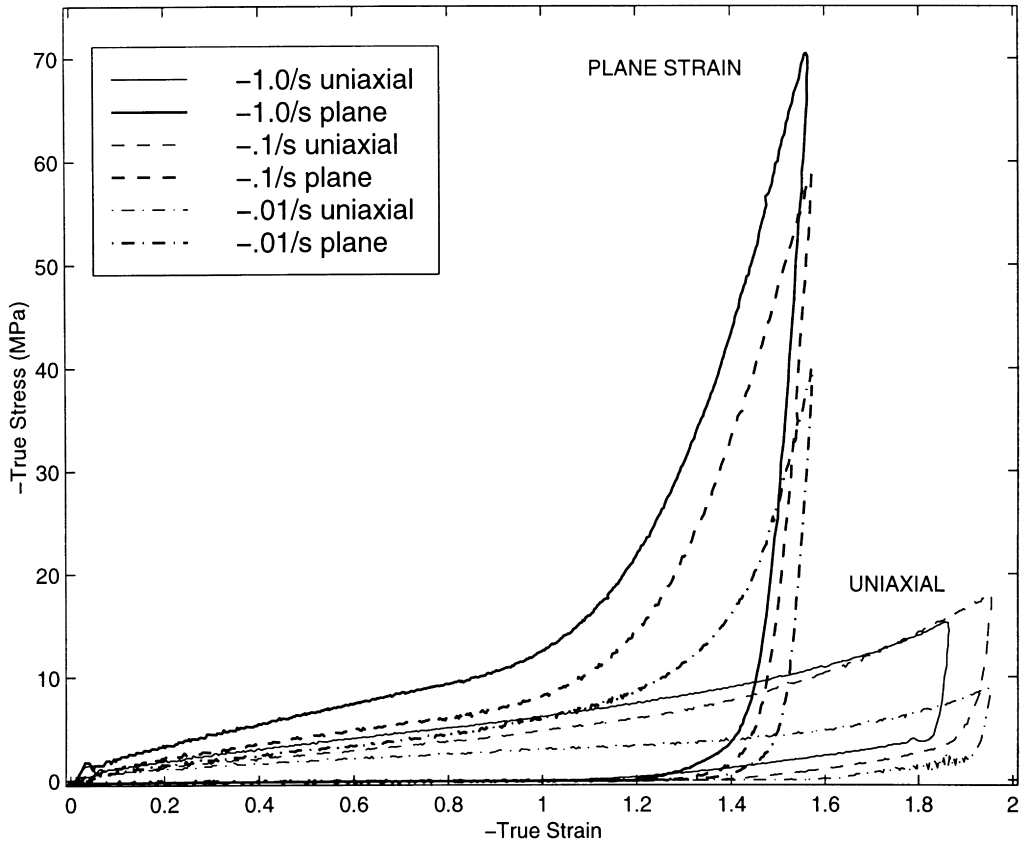

Fig. 10. True stress–strain behavior in uniaxial and plane strain compression at 90°C and different strain rates.

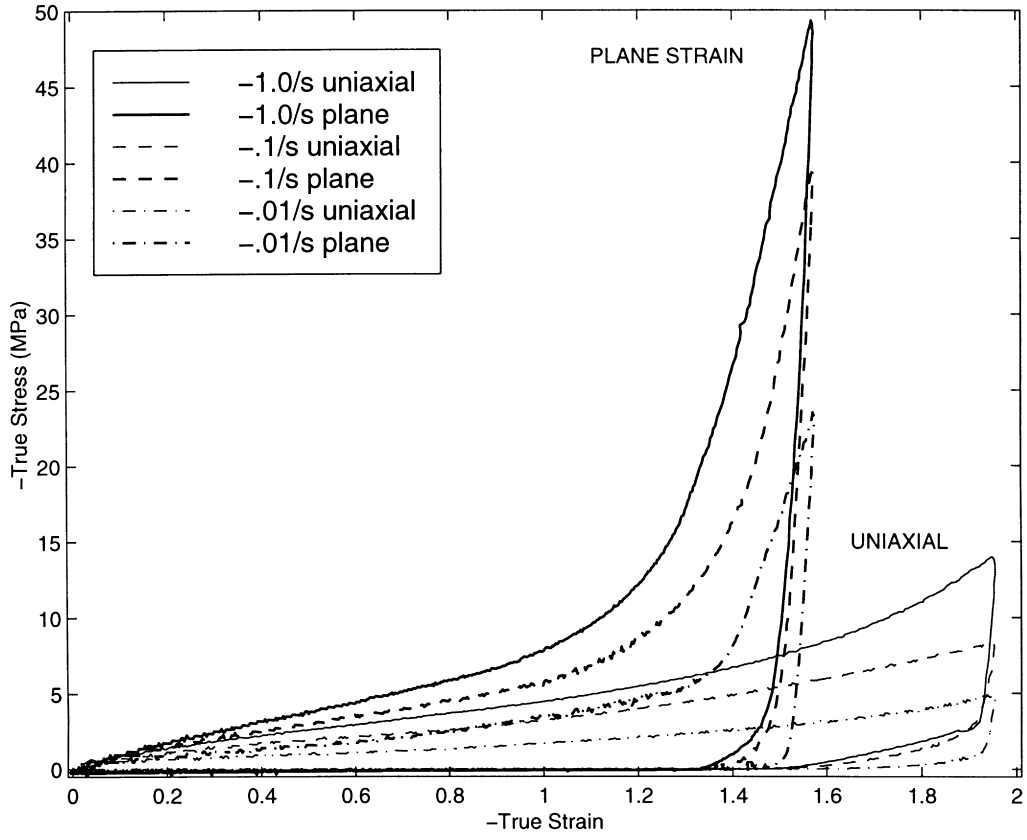

Fig. 11. True stress–strain behavior in uniaxial and plane strain compression at 100°C and different strain rates.

region, 90°C, 100°C and 105°C at strain rates of -0.1 and $-1.0\ s^{-1}$, respectively. It can be seen that as the deformation temperature increases the overall stress level decreases. Also, as the deformation temperature increases the amount of recovery upon unloading decreases, which was also the case with final unloaded specimens.

Figs. 6 and 7 show that all aspects of the stress–strain behavior depend on temperature. The initial flow stress decreases with increasing temperature; the strain at which the dramatic increase in hardening occurs increases with increasing temperature; the initial strain hardening slope decreases as the temperature is increased.

4.1.2. Plane strain compression tests

Fig. 8 shows the plane strain compression loading–unloading curves at different strain rates at a temperature of 90°C to a final strain of -1.6. The plane strain flow stress increases with increasing strain rate; the initial strain hardening slope increases as the strain rate is increased; the strain at which dramatic hardening occurs decreases with increasing strain rate.

Fig. 9 shows the plane strain compression at 90°C and 100°C at a strain rate of $-1.0\ s^{-1}$. The flow stress decreases with increasing temperature; the initial strain hardening slope decreases as the temperature is increased; the onset of dramatic strain hardening occurs at a larger strain as the temperature increases. It is also evident that as the deformation temperature increases, the strain level at which the unloading portion of the curves reaches zero stress decreases. This is a measure of the recovery of the specimen after loading and unloading. Therefore, as the deformation temperature increases, the amount of recovery upon unloading decreases.

4.1.3. Effects of state of strain

Figs. 10 and 11 show a direct comparison between uniaxial and plane strain compression in the rubbery region for strain rates of -1.0, -0.1, and $-0.01\ s^{-1}$ at deformation temperatures of 90°C and 100°C, respectively. It can be observed that for the same deformation conditions of temperature and strain rate, the plane strain compression stress is always greater than the uniaxial compression stress at any given strain. The initial flow stress in plane strain compression is higher than that in uniaxial compression owing to the plane strain constraint and can be simply explained in terms of a Mises yield criterion. It is also apparent from the figures that the strain hardening in plane strain is much more severe than in uniaxial compression. This is attributed to the difference in evolution in molecular orientation with strain for different states of strain and is also observed in polymers that remain amorphous with deformation. These results were also found by Arruda et al. [2] for poly(methylmethacrylate) and polycarbonate. Uniaxial compression produces an equi-biaxial state of

Table 2
Uniaxial compression data reduced from DSC thermograms

Mechanical test conditions	T_{cc} (°C)	p_{cr} (%)
As-received PET	137	10
Uniaxial, 90°C, $\dot{\varepsilon} = 0.0005\ s^{-1}$, $\varepsilon_f = -2.0$	104	31
Uniaxial, 90°C, $\dot{\varepsilon} = 0.1\ s^{-1}$, $\varepsilon_f = -2.0$	97	33
Uniaxial, 90°C, $\dot{\varepsilon} = -0.1\ s^{-1}$, $\varepsilon_f = -2.0$	100	27
Uniaxial, 100°C, $\dot{\varepsilon} = 0.005\ s^{-1}$, $\varepsilon_f = -2.0$	124	11
Uniaxial, 100°C, $\dot{\varepsilon} = 0.1\ s^{-1}$, $\varepsilon_f = -2.0$	104	26
Uniaxial, 100°C, $\dot{\varepsilon} = 1.0\ s^{-1}$, $\varepsilon_f = -2.0$	117	37
Uniaxial, 105°C, $\dot{\varepsilon} = 0.01\ s^{-1}$, $\varepsilon_f = -2.0$	109	14
Uniaxial, 105°C, $\dot{\varepsilon} = 0.1\ s^{-1}$, $\varepsilon_f = -2.0$	98	30
Uniaxial, 105°C, $\dot{\varepsilon} = 1.0\ s^{-1}$, $\varepsilon_f = -2.0$	108	36
Uniaxial, 105°C, $\dot{\varepsilon} = 2.0\ s^{-1}$, $\varepsilon_f = -2.0$	108	37

molecular orientation whereas plane strain compression produces a three-dimensional orientation that is dominated by molecular alignment in the FD. In the case of PET, this difference in strain hardening may also be attributable in part to strain-induced crystallization. The effects of deformation on the degree of crystallinity are evident from the DSC and WAXD measurements discussed in the following section.

The compression test results, more specifically the strain rate and temperature dependent behavior, obtained in this investigation are all consistent with basic trends of the mechanical behavior of PET as found by previous investigators in tensile tests such as Misra and Stein [6], Jabarin and coworkers [9,10], and Buckley et al. [11].

Table 3
Plane strain compression data reduced from DSC thermograms

Mechanical test conditions	T_{cc} (°C)	p_{cr} (%)
Plane strain, 90°C, $\dot{\varepsilon} = -0.01\ s^{-1}$, $\varepsilon_f = -1.6$	95	36
Plane strain, 90°C, $\dot{\varepsilon} = -0.1\ s^{-1}$, $\varepsilon_f = -1.0$	107	37
Plane strain, 90°C, $\dot{\varepsilon} = -0.1\ s^{-1}$, $\varepsilon_f = -1.2$	108	38
Plane strain, 90°C, $\dot{\varepsilon} = -0.1\ s^{-1}$, $\varepsilon_f = -1.4$	103	35
Plane strain, 90°C, $\dot{\varepsilon} = -0.1\ s^{-1}$, $\varepsilon_f = -1.6$	98	36
Plane strain, 90°C, $\dot{\varepsilon} = -1.0\ s^{-1}$, $\varepsilon_f = -1.6$	100	38
Plane strain, 90°C, $\dot{\varepsilon} = -0.2\ s^{-1}$, $\varepsilon_f = -1.6$	102	41
Plane strain, 100°C, $\dot{\varepsilon} = -0.01\ s^{-1}$, $\varepsilon_f = -1.6$	100	38
Plane strain, 100°C, $\dot{\varepsilon} = -0.1\ s^{-1}$, $\varepsilon_f = -1.6$	104	40
Plane strain, 100°C, $\dot{\varepsilon} = -1.0\ s^{-1}$, $\varepsilon_f = -1.6$	116	40
Plane strain, 100°C, $\dot{\varepsilon} = -2.0\ s^{-1}$, $\varepsilon_f = -1.6$	119	41

4.2. Results from differential scanning calorimetry measurements

DSC thermograms were taken on specimens in the as-received condition as well on specimens that had been loaded and unloaded in uniaxial and plane strain compression at different strain rates, to different final strains and at different temperatures. Table 2 summarizes the data calculated from the DSC thermograms taken on the as-received specimen and the uniaxial compression specimens by giving the onset of the cold crystallization exotherm, T_{cc}, and the weight percent crystallinity, p_{cr}.

Table 3 summarizes the data calculated from the DSC thermograms taken for the plane strain compression mechanical test specimens.

The glass transition temperature T_g of the as-received material, at a heating rate of 10°C min^{-1}, was observed at approximately 79°C. As the temperature is increased beyond T_g the material begins to crystallize in the DSC pan, where the onset of the cold crystallization exotherm, T_{cc}, was observed at 137°C at this heating rate and the area of cold crystallization, A_{cc}, was observed to be $-29\ J\ g^{-1}$. As the temperature increases, the crystals begin to melt at the onset of the melting endotherm, T_m, observed at 251°C. The melting continues through the melting endotherm, reaching a peak maximum at 258°C and having an area, A_m, of 41 J g^{-1}.

4.2.1. DSC trends in uniaxial compression

Table 2 shows the DSC results for various strain rates to a final strain of −2.0 at deformation temperatures of 90°C, 100°C, and 105°C. At a deformation temperature of 90°C, the different strain rates do not seem to have much of an effect on the percent crystallinity. The percent crystallinity is approximately 30% for all strain rates. This is not the case for deformation temperatures of 100°C and 105°C. At 100°C the crystallinity content increases with increasing strain rate and at 105°C the crystallinity content increases from 14% to 30% as the strain rate is increased by just one order of magnitude. This correlates with the stress–strain curves presented earlier in Figs. 2–4. Examination of the stress–strain curves in uniaxial compression at a deformation temperature of 90°C shown in Fig. 2 shows that, at all strain rates, the curves exhibit strong strain hardening. Also, the percent crystallinity at a strain rate of $-1.0\ s^{-1}$ exhibit strong strain hardening. Also, the percent crystallinity at a strain rate of $-1.0\ s^{-1}$ is less than the crystallinities at strain rates of −0.005 and $-0.1\ s^{-1}$ owing to the adiabatic heating effect. This is evident in the stress–strain curve in Fig. 2. The curve for $-1.0\ s^{-1}$ shows a decrease in the amount of

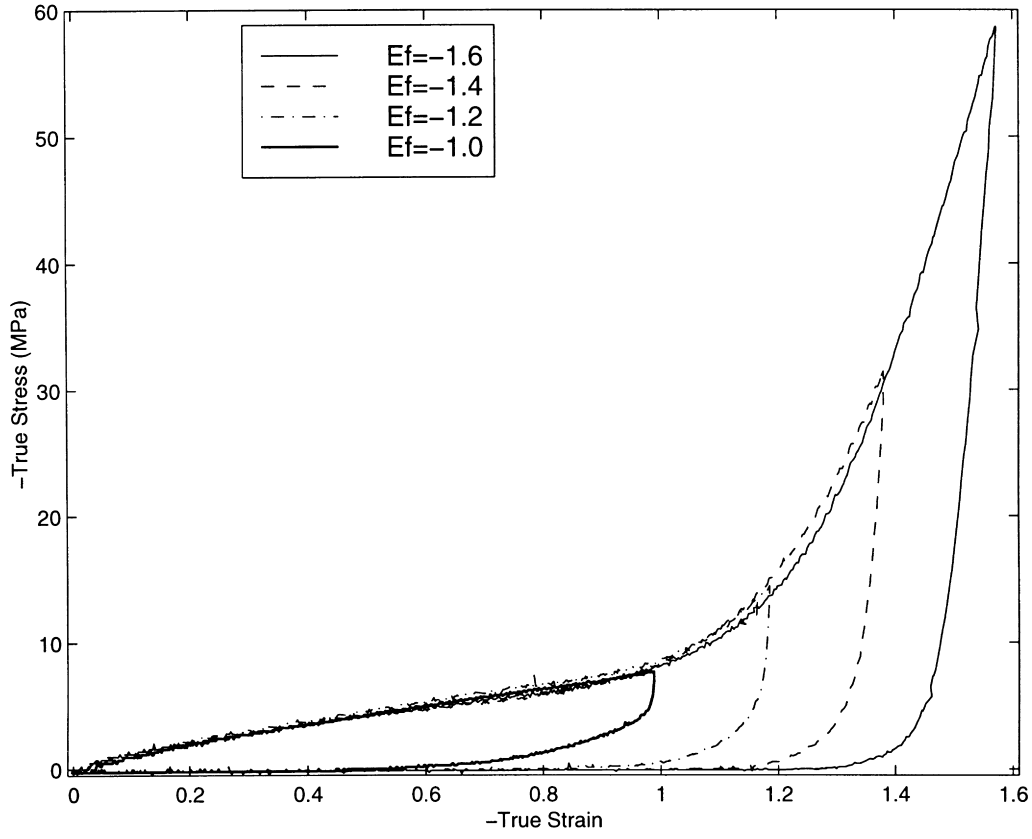

Fig. 12. True stress–strain behavior in plane strain compression at 90°C and −0.01/s showing loading and unloading to different strains.

strain hardening, thus manifesting itself as having lower percent crystallinity in the DSC thermogram. Fig. 3 shows the stress–strain curves that pertain to the DSC results for uniaxial compression performed at 100°C. At this temperature the crystallinity content increases for each increase in strain rate. This correlates to the strain hardening behavior in the stress–strain curves in Fig. 3. One can see an increase in the strain hardening slope as the strain rate increases from -0.005 to $-0.1\ s^{-1}$ and finally to $-1.0\ s^{-1}$. This manifests itself in the gradual increase in percent crystallinities at these strain rates. Fig. 4 shows the stress–strain curves that pertain to the DSC results for uniaxial compression performed at 105°C. At this temperature the crystallinity content is 14% for $-0.01\ s^{-1}$, which is not much greater than the as-received crystallinity of 10%. For the strain rate of $-0.1\ s^{-1}$, the crystallinity jumps to 30%, then for the strain rates of -1.0 and $-2.0\ s^{-1}$ the crystallinities are about the same at 36% and 37%, respectively. Again, this can be correlated to the slope of the strain hardening portion of the stress–strain curves which can be seen in Fig. 4. At a strain rate of $-0.01\ s^{-1}$ it can be seen that the curve does not exhibit the upturn that signals the level of strain hardening that is apparent in the curves at faster strain rates. Also, the fact that the stress–strain curves at strain rates of -2.0 and $-1.0\ s^{-1}$ are parallel explains why they have about the same percent crystallinity of 36% and 37%, respectively. The slope of the stress–strain curve at $-0.1\ s^{-1}$ is less than the slopes of the curves at -2.0 and $-1.0\ s^{-1}$, thus the percent crystallinity is lower.

In all of the DSC scans performed on the specimens deformed at 90°C, 100°C, and 105°C it is evident that the cold crystallization temperature decreases, as was also found by Zaroulis and Boyce [15].

4.2.2. DSC trends in plane strain compression

Table 3 shows the DSC results of the plane strain specimens deformed to a final strain of -1.6 at strain rates of -0.01, -0.1, -1.0, and $-2.0\ s^{-1}$ at deformation temperatures of 90°C and 100°C, respectively. It can be seen from these DSC results that the crystallinity content increased from the straining at all temperatures and that the increase in crystallinity as the strain rate is increased is very slight. Referring back to the stress–strain data, all curves showed the dramatic increase in strain hardening. It can be concluded that plane strain compression performed in the rubbery region to a final strain of -1.6 results in a large amount of strain-induced crystallization and that this crystallization increases very slightly as the strain rate increases and as the deformation temperature increases.

In order to determine if this large amount of strain-induced crystallization is dependent on the final strain imparted, an additional set of mechanical experiments were conducted. Fig. 12 shows the stress–strain curves for plane strain compression experiments performed at 90°C to

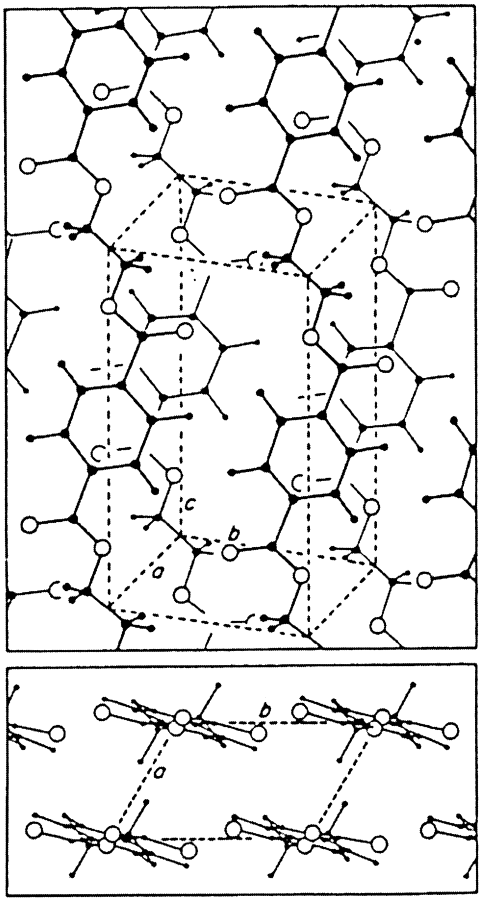

Fig. 13. Triclinic crystal structure of PET [23].

different levels of final strain of −1.0, −1.2, −1.4 and −1.6. Table 3 shows the DSC results of these experiments. It can be seen that even at a strain level as low as −1.0 the strain-induced crystallinity content is still about 37%. There is still ambiguity as to whether crystallization took place during straining or during the cool down period (i.e. an annealing effect). But, it is still observed that the strain-induced crystallization of PET occurs at a level of imparted strain lower than −1.0 in plane strain compression, where the stretch state for an imparted strain of −1.0 is $\lambda_1 = 0.37$, $\lambda_2 = 2.72$, and $\lambda_3 = 1.0$. This is consistent with the tensile stretching results of Misra and Stein [6], and Jabarin [9]. Misra and Stein stretched strips of amorphous PET above the glass transition temperature and found that strain-induced crystallization only occurred if the samples were stretched past 80% elongation. This is equivalent to 0.6 true strain. Jabarin stretched strips of PET to a final nominal strain of 1.1 at three different strain rates and found that the strain-induced crystallization occurs when samples are stretched to amounts below the strain hardening region of the force-extension curve.

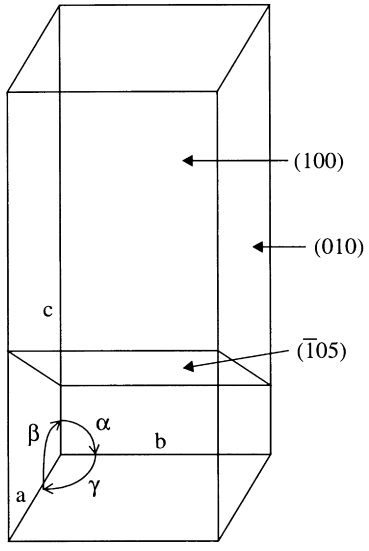

Fig. 14. PET triclinic unit cell structure with crystallographic slip planes.

4.3. Results from wide angle X-ray diffraction measurements

WAXD scans were taken on a specimen in the as-received condition as well as specimens that had been loaded and unloaded in uniaxial and plane strain compression at different strain rates, final strains and temperatures. Measurements were made in various deformation directions where the directions were defined earlier in Fig. 1. The WAXD scans enable the assessment of the nature and evolution of the texture, and thus the crystallinity, through comparison and analysis of the peaks corresponding to crystallographic planes.

The crystal structure of PET has a triclinic unit cell shown in Fig. 13 [23]. Fig. 14 shows the triclinic unit cell structure with the crystallographic diffracting planes. The unit cell parameters are $a = 0.45$ nm, $b = 0.59$ nm, $c = 10.7$ nm, $\alpha = 100°$, $\beta = 118°$ and $\gamma = 112°$ [24]. For PET, the diffraction peaks at $2\theta = 17°$, 26°, and 43° are identified with the crystallographic planes (0 1 0), (1 0 0), and, respectively. The other diffraction peaks that might be of interest in PET at $2\theta = 16°$, 21°, and 23° are identified with the crystallographic planes (0 $\bar{1}$ 0), (1 $\bar{1}$ 1), and ($\bar{1}$ 1 0), respectively.

The WAXD scan of an isotropic semi-crystalline PET in Fig. 15 [23] reveals a number of crystalline reflections. The PET specimen had been annealed at 190°C in order to crystallize the material. In Bellare et al. [23], the semi-crystalline PET was then highly textured via plane strain compression at 190°C. The WAXD scans of this fully textured semi-crystalline PET scanned perpendicular to the CD, FD, and LD directions are shown in Fig. 16 [23]. The scans in Fig. 16 reveal increased diffracted intensity of the (1 0 0), (0 1 0), and ($\bar{1}$ 0 5) planes in the three respective directions relative to the other crystal reflections. The LD scan indicates that the (1 0 0) plane is lying perpendicular to the LD, the CD scan indicates that the (0 1 0) plane is lying perpendicular to the constrained direction, and the FD scan indicates that the ($\bar{1}$ 0 5) plane is lying perpendicular to the

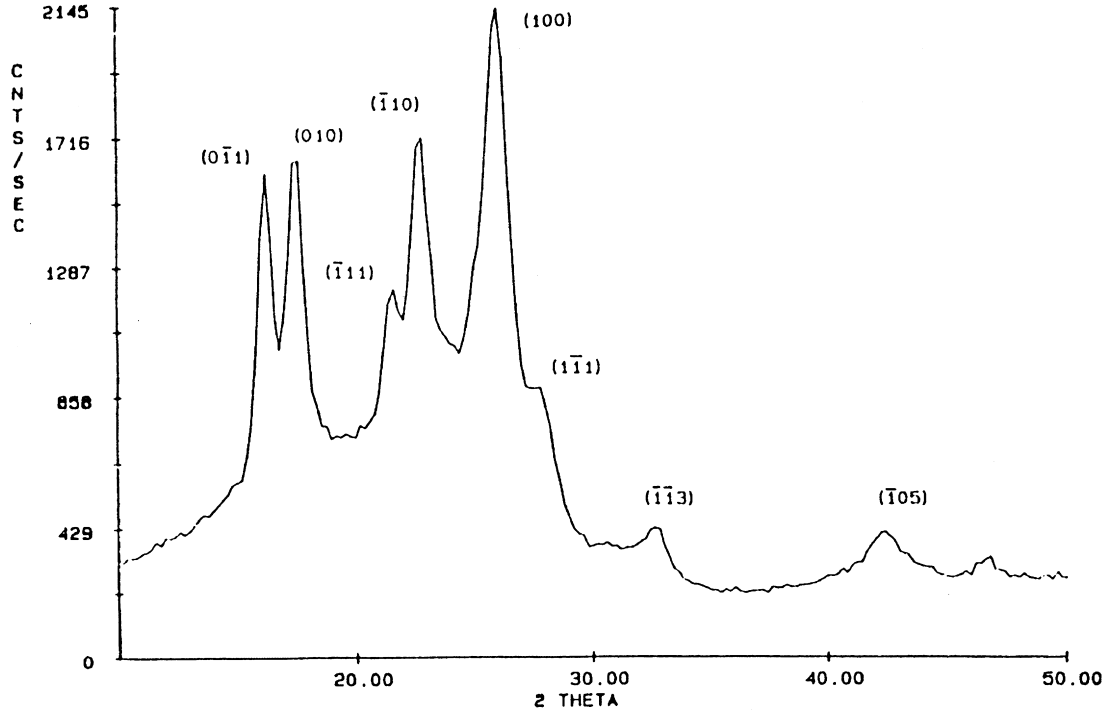

Fig. 15. WAXD scan of isotropic semi-crystalline PET [23].

FD. Figs. 15 and 16 will serve as a reference to the WAXD scans performed in this investigation.

Fig. 17 shows the WAXD scan of the isotropic as-received material showing only broad maxima as is characteristic of amorphous solids [25]. In Fig. 17, note that the scan in the FD is a scaled version of the scan in the LD because the FD scan is performed in reflection whereas the LD scan in performed is transmission.

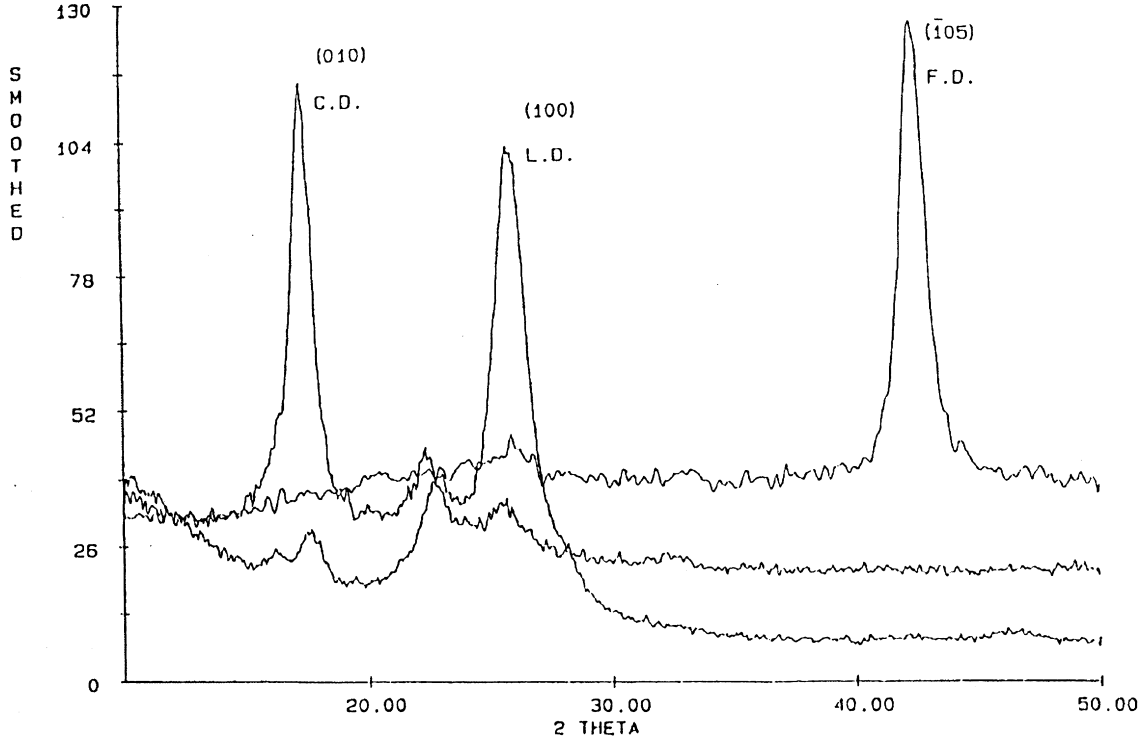

Fig. 16. WAXD scan of semi-crystalline PET as textured by plane strain compression [12].

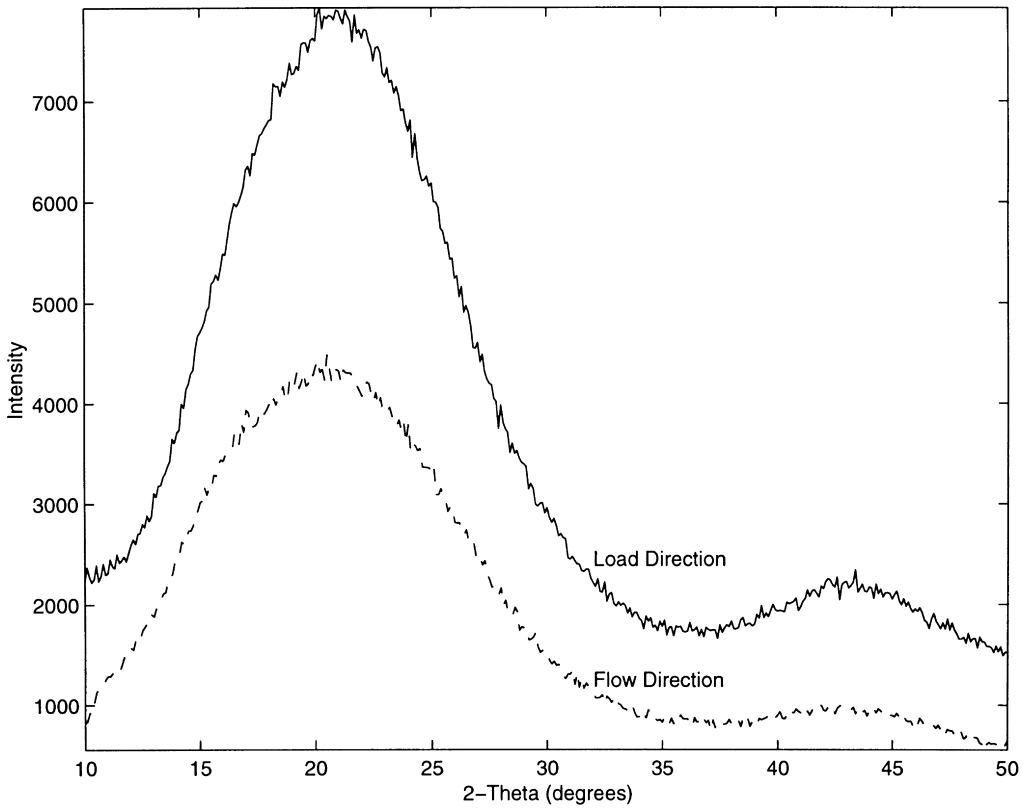

Fig. 17. WAXD scan of the as-received PET.

4.3.1. WAXD results in uniaxial compression

Fig. 18 shows the WAXD scans performed on specimens uniaxially compressed at 100°C to a final strain of −2.0 at strain rates of −0.005, −0.1, and −1.0 s^{-1}. As expected, the WAXD scans in any FD for specimens deformed in uniaxial compression were the same, therefore, only one WAXD scan in the FD is shown. In the figure, the evolution of the texture with increasing strain rate can be seen. The peaks become more defined and apparent, evolving from the amorphous oriented pattern at $-0.005\ s^{-1}$ to the peaks signifying crystallinity at $-1.0\ s^{-1}$. The deformation at 100°C results in the (1 0 0) planes of the crystals lying perpendicular to the LD, and the (0 1 0) planes of the crystals lying parallel to the LD. Fig. 19 schematically depicts how the crystals are oriented in a uniaxially compressed specimen that has undergone crystallization. The (1 0 0) planes of the crystals are oriented perpendicular to the LD, and the (0 1 0) and ($\bar{1}$ 0 5) planes are oriented randomly perpendicular to the FD. The development of this crystallographic texture is consistent with the development of molecular orientation in uniaxial compression. During uniaxial compression, a biaxial state of molecular orientation develops in the plane with increasing strain where the molecular chains align with the FD. The alignment of chains in the FD leads to the preferential crystallization where the crystal chain axis lies in the plane as shown in Fig. 19. Increased intensity of the prominent reflections is observed in specimens deformed at higher strain rates. This leads to the conclusion that the crystallinity increases as the strain rate increases. This is the same conclusion reached from the DSC results of the same specimens shown in Table 2 and is also consistent with the observed rate dependence of strain hardening at 100°C shown in Fig. 11.

4.3.2. WAXD results in plane strain compression

In Fig. 20 the WAXD scans of specimens deformed in plane strain compression at 90°C to a final strain of −1.6 at strain rates of −0.01, −0.1, and $-1.0\ s^{-1}$ are shown in the constrained, flow, and LDs, respectively. These WAXD scans show several prominent peaks clearly indicating the presence of crystallinity. The WAXD scans in Fig. 20 show a prominent (1 0 0) peak in the LD, a prominent (0 1 0) peak in the constrained direction (CD), and a prominent ($\bar{1}$ 0 5) peak in the FD. While this preferential crystallographic texture differs from that observed in specimens deformed by uniaxial compression, it is consistent with the manner in which molecular orientation develops under plane strain compression loading conditions where the molecular chains preferentially align in the FD. In the CD curve in Fig. 20, the (0 1 0) crystallographic reflection is very prominent, indicating that the (0 1 0) plane of the crystals is oriented perpendicular to the constrained direction. In the FD curve, the ($\bar{1}$ 0 5) crystallographic reflection is prominent, indicating that the ($\bar{1}$ 0 5) plane of the crystals is oriented

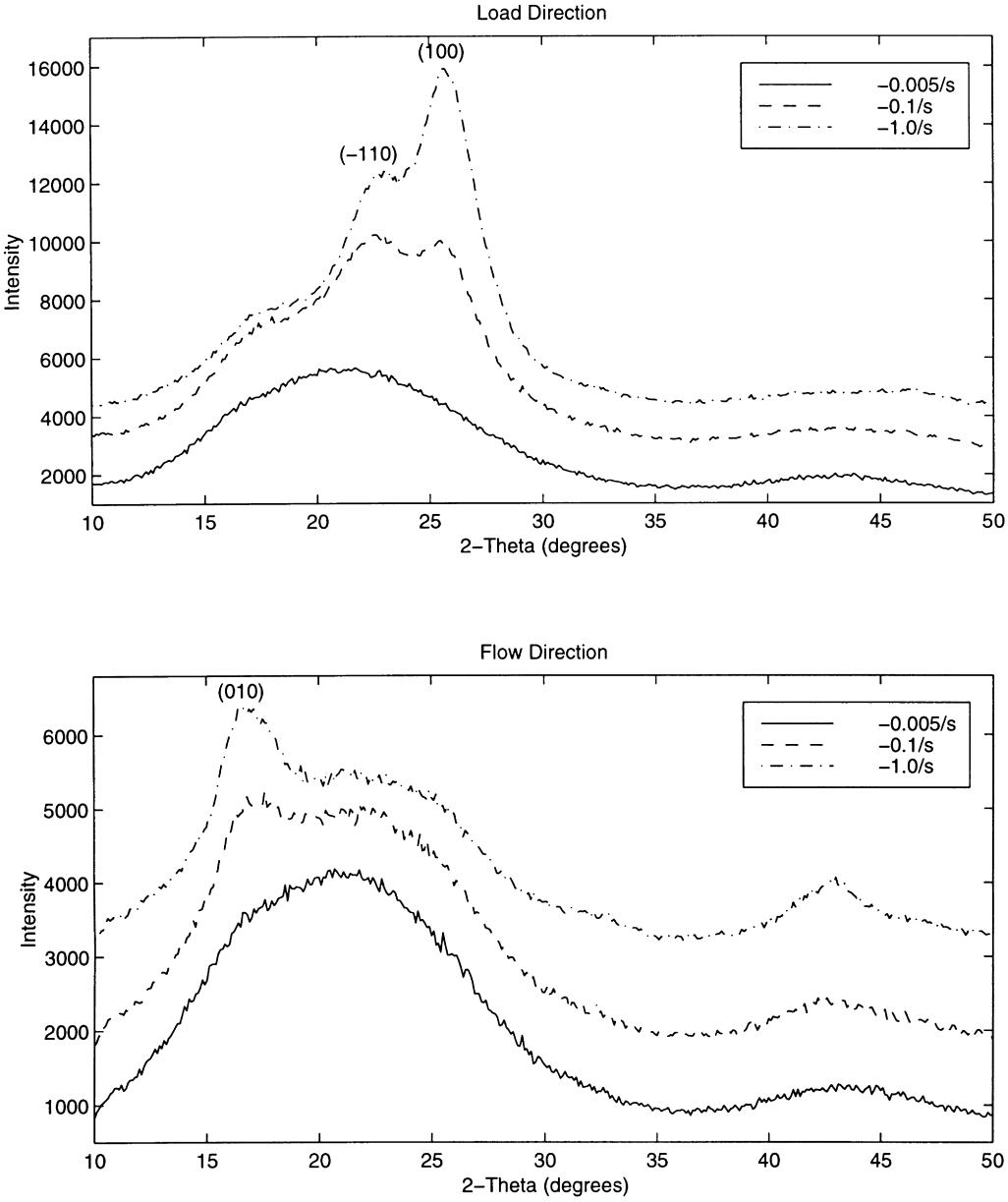

Fig. 18. WAXD scans of PET deformed in uniaxial compression to a strain of −2.0 at 100°C at different rates.

perpendicular to the FD. In the LD curve, the (1 0 0) crystallographic reflection is very prominent, indicating that the (1 0 0) plane of the crystals is oriented perpendicular to the LD. The crystallization in the preferential texture is shown in Fig. 21. The deformation results in the (1 0 0) plane lying perpendicular to the LD and parallel to the compression platens (making the aromatic ring in the plane of the sheet), the (0 1 0) plane lying perpendicular to the constrained direction and parallel to the walls of the channel die, and the ($\bar{1}$ 0 5) plane lying perpendicular to the FD and perpendicular to both the compression platens and the channel walls thus showing the chain direction of the crystals to be in the FD. The crystalline peaks become more defined and apparent as the strain rate is increased. The increase in strain rate results in more diffraction from crystallographic planes thereby increasing the intensity of these reflections. Thus Fig. 20 shows that the percentage crystallinity increases with increasing strain rate. This increase in crystallinity with increasing strain rate agrees with the DSC results shown in Table 3, although the WAXD scans show this increase in crystallinity more dramatically.

Fig. 22 shows the WAXD scans of specimens deformed in plane strain compression at 90°C at a strain rate of $-0.1\ s^{-1}$ to final strains of −1.0, −1.2, −1.4, and −1.6. As can be seen in the figure, the crystalline peaks become more defined and apparent as the strain is increased. The development of texture found in Fig. 20 for increasing strain rates also applies in this figure for increasing levels of final

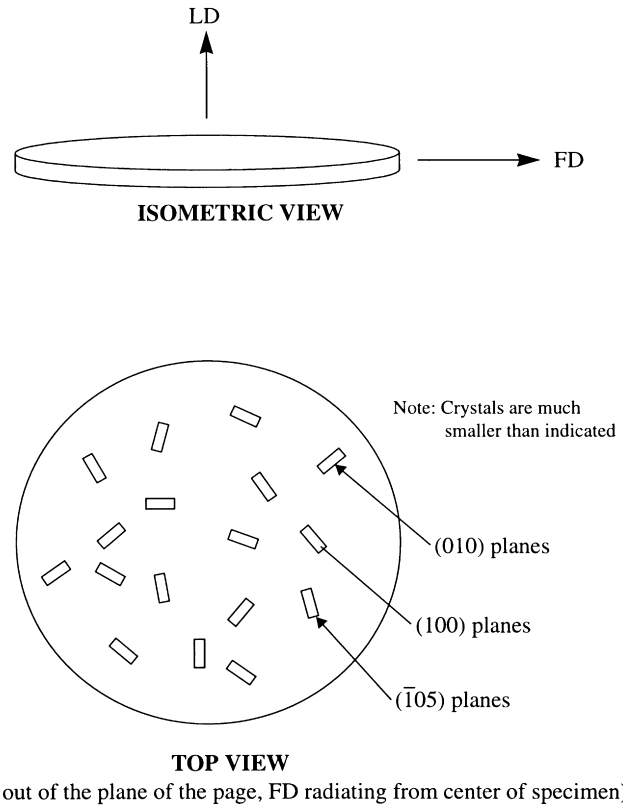

Fig. 19. Orientation of the crystals in specimens deformed in uniaxial compression; crystals are oriented with the (1 0 0) planes perpendicular to the load direction, and the (0 1 0) and (1 0 5) planes perpendicular to the page with their normals pointing in random directions parallel to the flow direction.

strain. The deformations result in the (1 0 0) plane of the crystals lying perpendicular to the LD, the (0 1 0) plane of the crystals lying perpendicular to the constrained direction, and the ($\bar{1}$ 0 5) plane of the crystals lying perpendicular to the FD. The increase in final strain level results in more diffraction from crystallographic planes thereby increasing the intensity of these reflections. Therefore, the crystallinity increases with increasing levels of final strain. This increase in crystallinity does not agree with the DSC results shown in Table 3. The discrepancy between the DSC results in Table 3 and their WAXD counterparts in Figs. 20 and 22 is most likely because of the difficulty in deciphering the cold crystallization area at high crystallinity content in the DSC scans. These cold crystallization peaks are very small and blend with the glass transition endothermic overshoot, making it difficult to measure their areas.

Fig. 23 shows the WAXD scans of specimens deformed in plane strain compression at a strain rate of $-0.1\ s^{-1}$ to a final strain of -1.6 at deformation temperatures of 90°C and 100°C. The scans show that the same basic crystallographic texture develops at both temperatures, however there are clear differences with respect to specific aspects of the texture. The specimens deformed at 90°C and 100°C exhibit well-defined peaks for both the (0 1 0) and ($\bar{1}$ 1 0) crystallographic reflections in the CD scans indicating that these planes in the crystals are oriented perpendicular to the constrained direction and that there is more diffraction from these planes as the deformation temperature is increased. In the LD scan, the (1 0 0) peak becomes more defined as the deformation temperature is increased, indicating that the (1 0 0) plane is oriented perpendicular to the LD and that there is more diffraction from this plane as the deformation temperature is increased. According to the DSC results for these specimens shown in Table 3, the crystallinities at these temperatures are 36% at 90°C and 40% for 100°C. This agrees with the WAXD scans with show that the peaks are more defined at 100°C than at 90°C. This trend is best observed in the LD scan.

A similar texture was observed in the WAXD scans of the initially semi-crystalline PET which had been textured by plane strain deformation shown earlier in Fig. 16. Although the two textures of Figs. 16 and 20 are similar, they were obtained by different processing routes. In Fig. 16, the material began in an isotropic semi-crystalline state and was then deformed. Therefore, the crystallographic texture had evolved from one of randomly oriented crystals to one of preferentially oriented crystals. Alternatively, in Fig. 20, the material began in an isotropic amorphous state. The deformation acted to preferentially orient the amorphous molecular network which then led to the crystallization, where the crystallization occurred in a preferential crystallographic orientation consistent with molecular orientation. Also, the preferential texture produced in plane strain compression shown in Fig. 20 is similar to the preferential

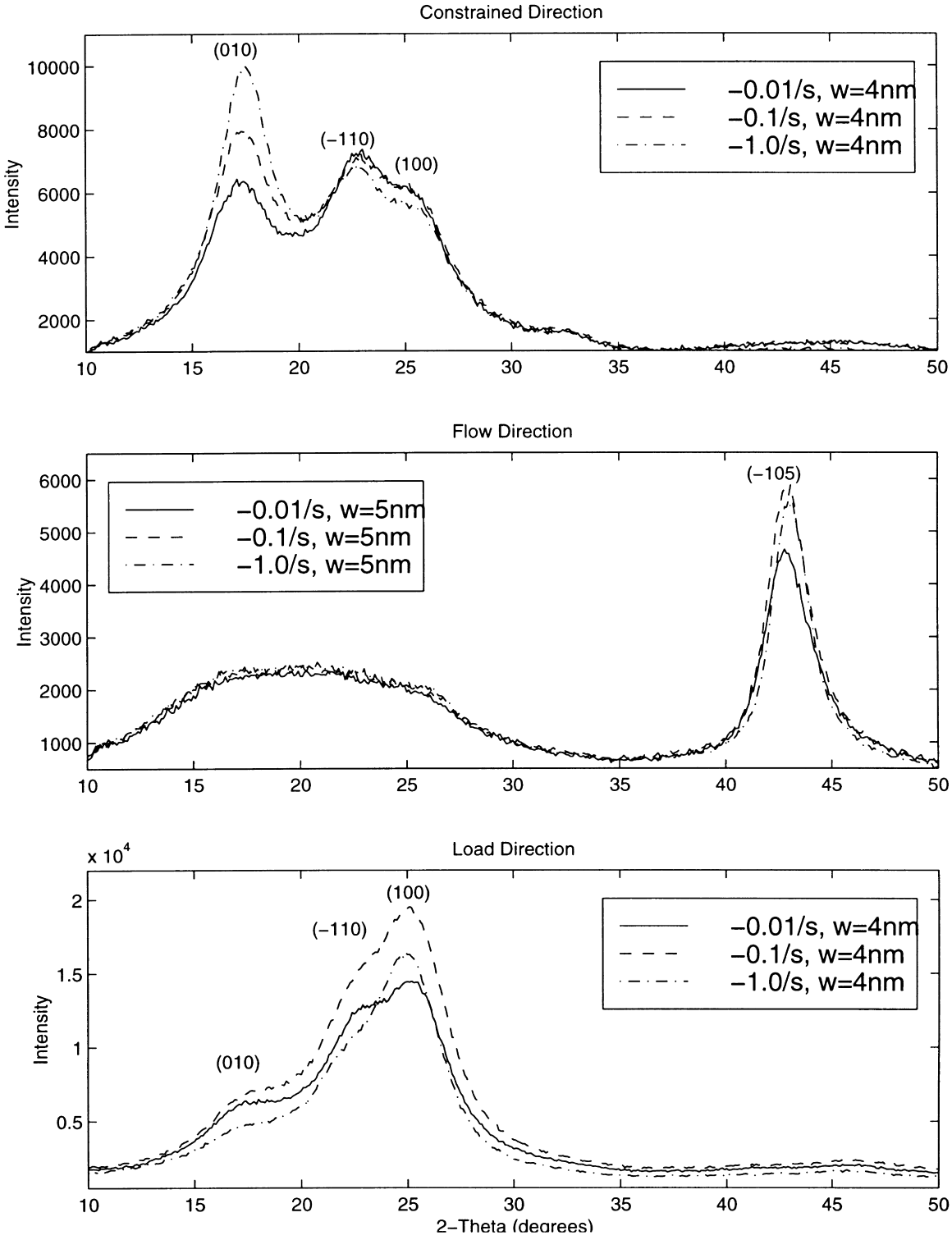

Fig. 20. WAXD scans of PET deformed in plane strain compression to a strain of −1.6 at 90°C and different strain rates.

texture produced in plane strain tension reported by Salem [14] indicating the importance of the stretch state in the structure development as opposed to the stress state. This conclusion had also been reached in the work of Guan et al. [8] as discussed earlier in Section 2.

The greater degree of texture resulting from plane strain compression than from uniaxial compression allowed the crystallite widths to be calculated from the WAXD scans in the three crystallographic directions for the plane strain compression specimens. The crystallite width is measured

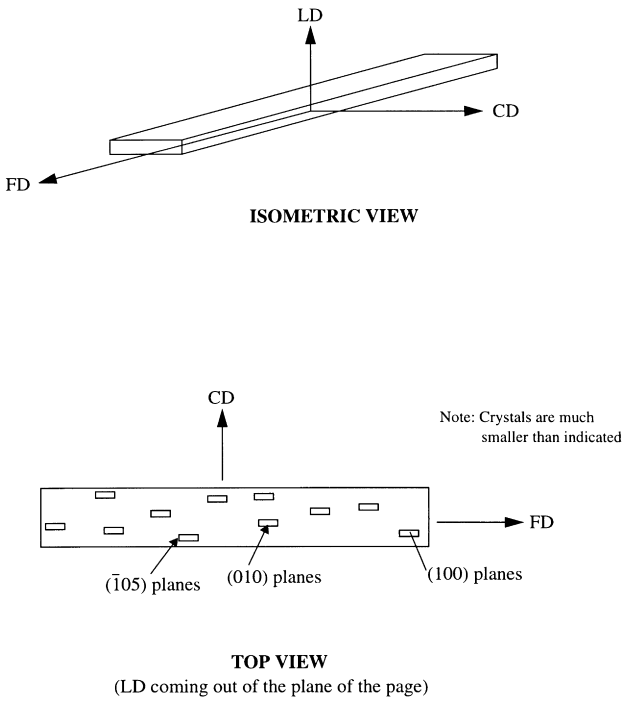

Fig. 21. Orientation of the crystals in specimens deformed in plane strain compression; crystals are oriented with the (1 0 0) planes perpendicular to the load direction, the (0 1 0) planes perpendicular to the constrained direction, and the (1 0 5) perpendicular to the flow direction.

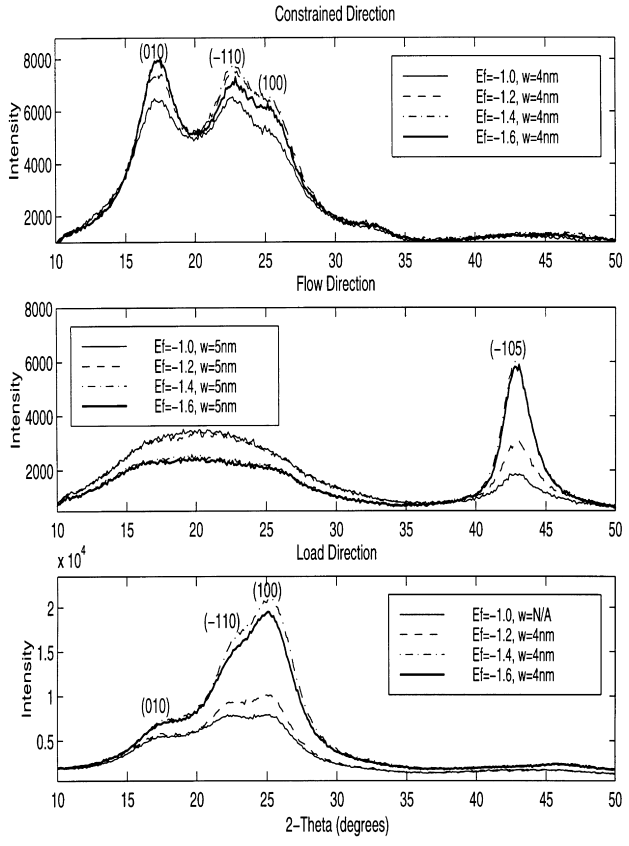

Fig. 22. WAXD scans of PET deformed in plane strain compression at 90°C and −0.1/s to different strains.

in a direction perpendicular to a particular set of reflecting planes. The width of the diffraction peak increases as the thickness of the crystallite decreases. The width of the crystallite can be calculated with the Scherrer equation [25]:

$$w = \frac{0.9\lambda}{B\cos\theta_B} \tag{6}$$

where $\lambda = 1.54$ nm is the wavelength of the X-rays, B is the full width at half peak maximum (also known as FWHM), and θ_B is the Bragg angle. After WAXD scans were taken on the plane strain specimens, JADE, a data analysis software package for X-ray diffraction curves, was used to determine B and θ_B. Using the values of B and θ_B from JADE, the crystallite widths could be calculated. In the WAXD scans for the plane strain specimens, the (0 1 0) plane was most evident in the CD scan, the ($\bar{1}$ 0 5) plane was most evident in the FD scan, and the (1 0 0) plane was most evident in the LD scan, therefore the crystallite width corresponding to each plane was calculated using the appropriate scan. Before discussing the WAXD scans performed for this investigation, it is important to review the reference scans in Figs. 15 and 16 of isotropic semi-crystalline PET and fully textured semi-crystalline PET, respectively. A rough estimate of the crystallite widths was calculated from these WAXD scans. For the isotropic case, the crystallite width is about 12 nm in the (1 0 0) plane and also about 12 nm in the (0 1 0) plane. The peak for the ($\bar{1}$ 0 5) plane is barely discernible to calculate a crystallite width. For the fully textured case, the crystallite width is about 10 nm in the (1 0 0) plane, about 15 nm in the (0 1 0) plane and about 13 nm in the ($\bar{1}$ 0 5) plane.

Fig. 20 shows the crystallite widths as a function of strain rate and scan direction, for specimens deformed at 90°C to a final strain of −1.6. For each of the scan directions, the crystallite widths are about the same regardless of strain rate. This shows that the increasing crystallinity with increasing strain rate, as evidenced by the increasing peak definition with increasing strain rate discussed earlier and by the DSC results in Table 3, is because of an increase in the number of crystallites rather than an increase in the size of the crystallites.

Fig. 22 shows the crystallite widths as a function of final strain level and scan direction for specimens deformed at 90°C at a strain rate of $-0.1\,s^{-1}$. For each of the scan directions, the crystallite widths are about the same regardless of strain level. This also shows that the increase in crystallinity with increasing strain level, as evidenced by the increasing peak definition with increasing strain level discussed earlier, is also owing to an increase in the number of crystallites rather than an increase in the size of the crystallites.

Fig. 23 shows the crystallite widths as a function of deformation temperature and scan direction for specimens deformed at a strain rate of $-0.1\,s^{-1}$ to a final strain of −1.6. The figure shows that the crystallite widths for the 100°C specimens differ markedly from the crystallite widths

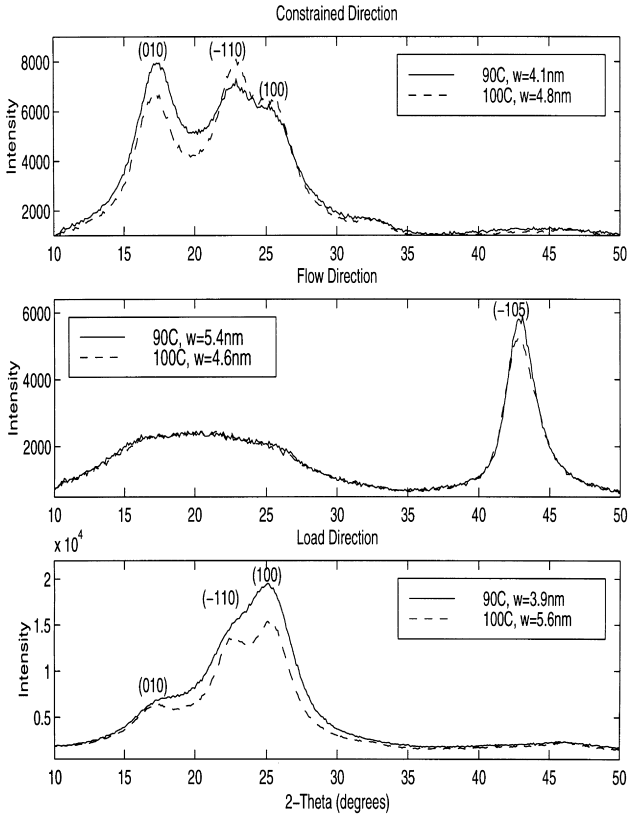

Fig. 23. WAXD scans of PET deformed in plane strain compression to a strain of −1.6 at −0.1/s and at 90°C, 100°C.

for 90°C specimens. It seems that at 100°C, the crystallite widths are greater in the (0 1 0) and (1 0 0) planes, but smaller in the ($\bar{1}$ 0 5) plane when compared to 90°C. This seems to suggest that, well into the rubbery region, the crystallite size changes as the deformation temperature is increased and that this change is characterized by an increase in the crystallite width in the (0 1 0) and (1 0 0) planes but a decrease in the crystallite width in the ($\bar{1}$ 0 5) plane.

The crystallite widths found in Figs. 20, 22 and 23 are in agreement with the range of crystallite widths found by Salem [14] and Peszkin and Schultz [26]. Peszkin and Schultz [26] found the crystallite widths in PET fibers that had been annealed for different lengths of time at 100°C under tension to be in the range of 3–5 nm. Salem [14] found the crystallite widths in PET films that had been stretched at 90°C at different strain rates to be 2.3–3.0 nm normal to the (1 0 0) planes and 2.8–4.0 nm normal to the (0 1 0) planes.

5. Discussion and conclusions

The mechanical tests and the microstructural analyses conducted by DSC and WAXD show that the mechanical behavior and structural evolution of PET is a strong function of deformation temperature, strain rate and strain state. The following trends can be observed from the data shown in the previous sections.

The stress–strain behavior of PET above the glass transition temperature exhibits four characteristic features: a relatively stiff initial response, followed by a rollover to a yield or flow-like behavior, followed by a gradual increase in stress with strain which is termed the initial strain hardening response, followed by a dramatic increase in stress with strain at large strains. The stiff initial response was only weakly dependent on strain rate, strain state and temperature. The stress at which the yield rollover occurred increased with increasing strain rate and decreasing temperature. The initial strain hardening slope increased with increasing strain rate and decreasing temperature and was greater in plane strain compression then in uniaxial compression at the same level of strain. Dramatic strain hardening occurred at smaller strain levels as the strain rate was increased and the temperature was decreased and the strain hardening was much more dramatic in plane strain compression than in uniaxial compression reaching greater overall stress levels.

DSC scans showed that the percent crystallinity increased with increasing strain rate and increasing temperature in the cases where heating effects were small. The DSC scans also showed that the percent crystallinity developed under plane strain compression was greater than that under uniaxial compression. These results were consistent with the trends found in the stress–strain curves, where the amount of dramatic strain hardening was an indication of the degree of crystallinity.

The WAXD scans showed the evolution of the texture that results in both uniaxial compression and plane strain compression. The WAXD scans were also consistent with the stress–strain results and the DSC results by showing that the degree of crystallinity increased with increasing strain rate and that the degree of crystallinity resulting from plane strain compression is more than that resulting from uniaxial compression. The WAXD scans also demonstrated that there is a difference in the resulting crystallographic textures between uniaxial compression and plane strain compression. In plane strain compression, the crystals lie in all three directions in the same orientation, whereas, in uniaxial compression, the crystals lie in only one direction in the same orientation, the LD, and lie randomly in the other two directions. However, in both cases, the chain axis is in the direction of flow.

The strain rate, strain state and temperature dependence of the material behavior of PET play an integral role during the processing of the material. It is important to investigate and be able to predict the mechanical behavior of the material in order to reduce cost and material waste. Therefore, it is important that a constitutive model of the mechanical behavior of the material be able to capture of the essence of the strain rate, strain state and temperature dependencies. In a separate paper, development of a constitutive model which captures these dependencies is proposed.

Acknowledgements

This research was funded by the National Science Foundation through award numbers MSS-9215805 and CMS-9622526 and by the Eastman Kodak Company. We are grateful to Mr. Arthur Buettner of the Eastman Kodak Company for supplying all materials. This work made use of MRSEC Shared Facilities supported by the National Science Foundation under Award Number DMR-9400334.

Appendix A

In the uniaxial compression experiments, the dominant mode of heat transfer during the course of the experiments is the conduction of heat from the uniaxially compressed sample to the compression platens. Let h_{inst} be the instantaneous height of the specimen during a compression experiment. Then the characteristic length that controls the heat transfer is the distance from the platen to the center of the specimen, which is half the current specimen height, $h_{char} = h_{inst}/2$. Thus, the time required for heat to conduct out of the sample, t_{cond}, is given as:

$$t_{cond} = \frac{(h_{char}/2)^2}{2\kappa/\rho c} \tag{A.1}$$

where $\kappa = 0.218\ \mathrm{W\,mK^{-1}}$ is the thermal conductivity, $\rho = 1330\ \mathrm{g\,cm^{-3}}$ is the density of amorphous PET, and $c = 1300\ \mathrm{J\,kg^{-1}\,K^{-1}}$ is the specific heat capacity.[1] For a constant strain rate test the loading time required to reach the final strain, t_{exp}, can be calculated by dividing the final strain, $\epsilon_f = -2.0$ by the strain rate, $\dot{\varepsilon}$.

References

[1] Marshall I, Thompson AB. The drawing of terylene. Journal of Applied Chemistry 1954;4:145–153.
[2] Arruda EM, Boyce MC, Jayachandran R. Effects of strain rate, temperature and thermo-mechanical coupling on the finite strain deformation of glassy polymers. Mechanics of Materials 1995;19:193–212.
[3] Thompson AB. Strain-induced crystallization of polyethylene terephthalate. Journal of Polymer Science 1959;34:741–759.
[4] Ward IM. The mechanical behavior of poly(ethylene terephthalate). Journal of Macromolecular Science 1967;4:667–694.
[5] Duckett RA, Rabinowitz S, Ward IM. The Strain-rate, temperature and pressure dependence of yield of isotropic poly(methylmethacrylate) and poly(ethylene terephthalate). Journal of Materials Science 1970;5:909–915.
[6] Misra A, Stein RS. Stress-induced crystallization of poly(ethylene terephthalate). Journal of Polymer Science: Polymer Physics Edition 1979;17:235–257.
[7] Ghanem AM, Porter RS. Cold crystallization and thermal shrinkage of uniaxially drawn poly(ethylene 26-naphthalate) by solid-state coextrusion. Journal of Polymer Science: Part B: Polymer Physics 1989;27:2587–2603.
[8] Guan JY, Wang L, Porter RS. Planar deformation of amorphous poly(ethylene terephthalate) by stretching and forging. Journal of Polymer Science: Part B: Polymer Physics 1992;30:687–691.
[9] Jabarin SA. Strain-induced crystallization of poly(ethylene terephthalate). Polymer Engineering and Science 1992;32:1341–1349.
[10] Chandran P, Jabarin S. Biaxial orientation of poly(ethylene terephthalate). Part I: nature of the stress–strain curves. Advances in Polymer Technology 1993;12:119–132.
[11] Buckley CP, Jones DC, Jones DP. Hot-drawing of poly(ethylene terephthalate) under biaxial stress: application of a three-dimensional glass-rubber constitutive model. Polymer 1996;37:2403–2414.
[12] Adams AM, Buckley CP, Jones DP. Biaxial hot-drawing of poly(ethylene terephthalate: dependence of yield stress on strain-rate ratio. Polymer, accepted for publication.
[13] Buckley CP, Salem DR. Polymer 1987;28:69.
[14] Salem DR. Development of crystalline order during hot-drawing of poly(ethylene terephthalate) film: influence of strain rate. Polymer 1992;33:3182–3188.
[15] Zaroulis JS, Boyce MC. Temperature, strain rate, and strain state dependence of the evolution in mechanical behavior and structure of poly(ethylene terephthalate) with finite strain deformation. Polymer 1997;38:1303–1315.
[16] Blundell DJ, MacKerron DH, Fuller W, Mahendrasingam A, Martin C, Oldman RJ, Rule RJ, Riekel C. Characterization of strain-induced crystallization of (poly ethylene terephthalate) at fast draw rates using synchrotron radiation. Polymer 1996;37:3303–3311.
[17] Mahendrasingam A, Martin C, Fuller W, Adams AM, Buckley CP, Blundell DJ, Jones DP, MacKerron DH. Structural changes and stress relaxation following drawing of PET. Tenth International Conference on Deformation, Yield and Fracture of Polymers, Churchill College, Cambridge, UK, 1997. p. 45–48.
[18] Arruda EM, Boyce MC. An experimental and analytical investigation of the large strain compressive and tensile response of glassy polymers. Polymer Engineering and Science 1990;30:1288–1298.
[19] Hasan OA, Boyce MC. A constitutive model for the nonlinear viscoelastic viscoplastic behavior of glassy polymers. Polymer Engineering and Science 1995;35:331–344.
[20] Polymer handbook, 3rd ed. New York: Wiley, 1989.
[21] Hasan OA, Boyce MC. Energy storage during inelastic deformation of glassy polymers. Polymer 1993;34:5085–5092.
[22] Blundell DJ, Beckett DR, Willcocks PH. Routine crystallinity measurements of polymers by d.s.c. Polymer 1981;22:704–707.
[23] Bellare A, Cohen RE, Argon AS. Development of texture in poly(ethylene terephthalate) by plane-strain compression. Polymer 1993;34:1393–1403.
[24] Encyclopedia of polymer science engineering. 2nd ed. New York: Wiley, 1985.
[25] Cullity BC. Elements of X-ray diffraction. 2nd ed. Massachusetts: Addison-Wesley, 1978.
[26] Peszkin PN, Schultz JM. Kinetics of fiber heat treatment. II. Poly(ethylene terephthalate) fibers. Journal of Polymer Science: Part B: Polymer Physics 1986;24:2591–2616.

[1] Property values extracted from the Polymer Handbook [20].